



**HAL**  
open science

## Geochemical variability in a single flow from northern Iceland

J. Maclennan, D. Mckenzie, F. Hilton, K. Gronvöld, N. Shimizu

► **To cite this version:**

J. Maclennan, D. Mckenzie, F. Hilton, K. Gronvöld, N. Shimizu. Geochemical variability in a single flow from northern Iceland. *Journal of Geophysical Research: Solid Earth*, 2003, 108, p. 289-310. 10.1029/2000JB000142 . insu-03598431

**HAL Id: insu-03598431**

**<https://insu.hal.science/insu-03598431>**

Submitted on 5 Mar 2022

**HAL** is a multi-disciplinary open access archive for the deposit and dissemination of scientific research documents, whether they are published or not. The documents may come from teaching and research institutions in France or abroad, or from public or private research centers.

L'archive ouverte pluridisciplinaire **HAL**, est destinée au dépôt et à la diffusion de documents scientifiques de niveau recherche, publiés ou non, émanant des établissements d'enseignement et de recherche français ou étrangers, des laboratoires publics ou privés.

Copyright

## Geochemical variability in a single flow from northern Iceland

J. Maclennan,<sup>1</sup> D. McKenzie, and F. Hilton

Bullard Laboratories, Department of Earth Sciences, Cambridge, UK

K. Gronvöld

Nordic Volcanological Institute, Reykjavik, Iceland

N. Shimizu

Department of Geology and Geophysics, Woods Hole Oceanographic Institution, Woods Hole, Massachusetts, USA

Received 9 January 2001; revised 24 June 2002; accepted 19 August 2002; published 4 January 2003.

[1] Compositional variability is present for almost every element analyzed in 70 whole rock samples and 40 olivine-hosted melt inclusions from the Borgarhraun lava flow in NE Iceland. The variation of incompatible element concentrations can be produced by incomplete mixing of fractional melts, while the compatible element variations in the whole rock samples can be explained by addition/removal of crystals found in the flow. The melt inclusion incompatible element compositions are more variable than the whole rock compositions, and the magnitude of variability of the whole rock samples can be matched if each hand specimen is made of magma that was formed by mixing of 20–30 batches of melt with the composition of the inclusions. Clinopyroxene barometry and the major element composition of the whole rock samples suggest that mixing took place at pressures of  $\sim 0.9$  GPa in sub-Moho magma chambers. The spatial distribution of the concentrations of incompatible elements is not random in Borgarhraun and samples with a separation of  $<4$  km have concentrations that are more similar than expected from a random distribution of geochemistry. This separation distance corresponds to a lava volume of  $0.014$ – $0.14$  km<sup>3</sup>. This volume may be controlled by magma mixing and episodic eruption of melts from a sub-Moho chamber. The concentration variations of compatible elements with position in the flow are little different to those expected for random variation. It is likely that the crystal removal and addition processes that control major element compositions generate variability on short length scales. *INDEX TERMS:* 3640 Mineralogy and Petrology: Igneous petrology; 8439 Volcanology: Physics and chemistry of magma bodies; 3655 Mineralogy and Petrology: Major element composition; 3670 Mineralogy and Petrology: Minor and trace element composition; *KEYWORDS:* Iceland, basalt, geochemical variability, magma mixing

**Citation:** Maclennan, J., D. McKenzie, F. Hilton, K. Gronvöld, and N. Shimizu, Geochemical variability in a single flow from northern Iceland, *J. Geophys. Res.*, 108(B1), 2007, doi:10.1029/2000JB000142, 2003.

### 1. Introduction

[2] If the composition of lava erupted at the Earth's surface is representative of magma generated in the melting region, then it is possible to use the lava composition to investigate mantle melting. Therefore the assumption that melts are perfectly mixed before eruption is built into most models of melt generation, and it is often necessary to assume that a small number of lava samples can be used to characterize the melting under long stretches of the mid-ocean ridge system [e.g., White *et al.*, 1992]. However, it is well known from studies of melt inclusions that

small-scale geochemical variability is preserved in primitive mid-ocean ridge basalt (MORB). The rare earth element (REE) concentrations of melt inclusions trapped in crystals from single samples have been found to be variable [Nielsen *et al.*, 1995; Gurenko and Chaussidon, 1995; Shimizu, 1998; Kamenetsky *et al.*, 1998], along with the compositions of melt inclusions contained in single crystals [Nielsen *et al.*, 1995; Kamenetsky *et al.*, 1998; Slater *et al.*, 2001]. Furthermore, studies of the Theistareykir volcanic system in NE Iceland have shown that short length-scale variability exists in the incompatible element compositions of lava samples [Elliott *et al.*, 1991; Slater *et al.*, 2001]. Therefore the perfect mixing assumption of the melting models is not correct in detail and more information about the melt mixing process is required in order to assess the significance of the results of the melting models.

<sup>1</sup>Now at Laboratoire de Géosciences Marines, Institut de Physique du Globe de Paris, Paris, France.

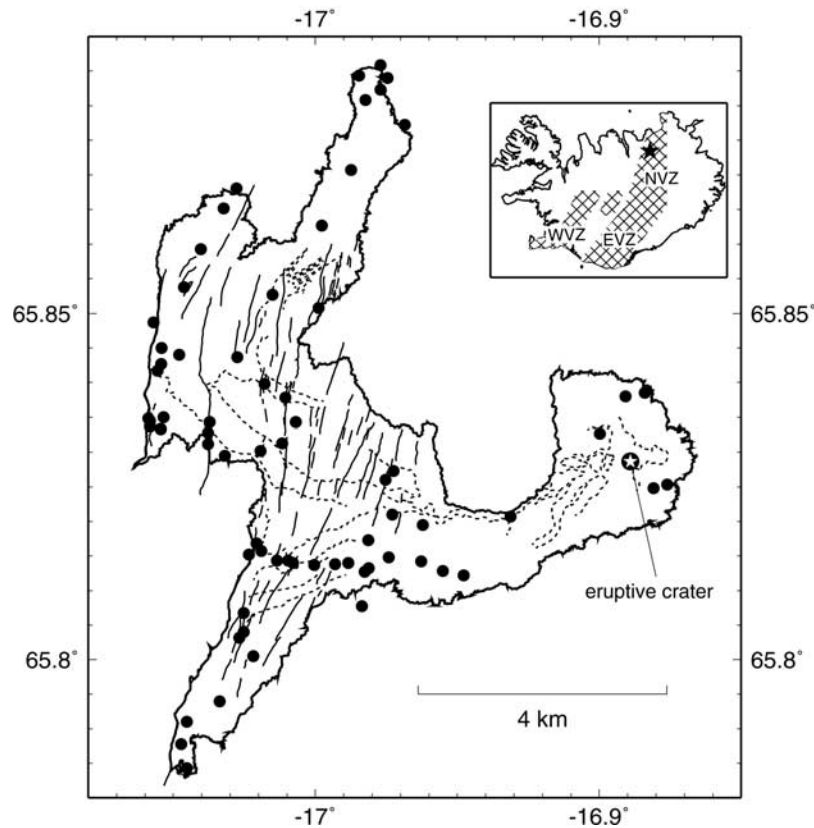


**Figure 1.** Map of Borgarhraun. Sample positions are solid circles, channel margins are dotted lines, faults are thin solid lines. The crater position is marked as a star inside a circle. Inset map shows approximate position of Borgarhraun in Iceland. Borgarhraun is marked by the star and sits at the northern end of the Northern Volcanic Zone (NVZ). Hatched areas show volcanic zones.

[3] The aim of this study is to provide information about the extent and location of mixing and the associated length scales of variability by study of the geochemical variation within a single lava flow. Detailed sampling of single flows on submerged parts of the mid-ocean ridge system is difficult and expensive [Perfit and Chadwick, 1998; Rubin *et al.*, 2001], so most studies of variability within flows have been limited to ocean islands such as Hawaii [Rhodes, 1983] and Iceland [Watkins *et al.*, 1970; Lindstrom and Haskin, 1981; Sigmarsson *et al.*, 1991]. The only detailed study of compositional variability in a single recent flow from Iceland to date is that of the 1783–1784 Lakagigar eruption in southern Iceland [Sigmarsson *et al.*, 1991]. This is the second largest recorded historical eruption on Iceland, with a volume of  $\sim 15 \text{ km}^3$ . Sigmarsson *et al.* presented U and Th contents for 11 whole rock and tephra samples and concluded that the flow was compositionally uniform for these trace elements. No other elemental concentrations were reported. Since the Lakagigar magma is a relatively evolved basalt, Sigmarsson *et al.* proposed that the melt composition was homogenized by mixing in a large magma chamber. It is possible that more primitive flows than Lakagigar will have spent less time in magma chambers and will not be as geochemically homogeneous. One such flow is Borgarhraun, from the Theistareykir

volcanic system, and this flow was selected for detailed study.

## 2. Sample Collection and Description

[4] Mapping and geochemical studies of the Theistareykir volcanic system have shown that it contains a number of primitive flows [O'Nions *et al.*, 1976; Elliott *et al.*, 1991; Slater *et al.*, 2001]. The Borgarhraun flow was chosen because the work of Slater [1996] indicated that compositional variability was present in the Borgarhraun samples and in melt inclusions hosted by crystals carried in the flow. Borgarhraun has an average MgO content of  $\sim 12 \text{ wt } \%$ , which is slightly lower than that expected for unmodified mantle melts. Olivine, clinopyroxene and plagioclase crystals are visible in most hand specimens of Borgarhraun lava. Tephrochronology has been used to date the flow at between 10.5 and 7 kyr B.P. [Sæmundsson, 1991] and the surface area of the flow is  $\sim 35 \text{ km}^2$ . A total of 77 samples was collected from Borgarhraun over a period of 10 days during August 1998. The surface of the flow is almost completely exposed and samples were taken from positions fairly evenly distributed across the flow, giving an average distance from a sample to its nearest neighbor of  $\sim 323 \pm 25 \text{ m}$  (Figure 1). Aerial photographs and field mapping show that the flow

was erupted from a crater near the easternmost point of Borgarhraun. While a small volume of lava spilled over the crater edge to the east, most of the lava flowed westward down a gentle slope to the edge of a graben. Inside the graben, several channels fed lava to the north, while in at least one case a channel diverted lava to the south. Most of the surface area of Borgarhraun is composed of flow lobes that were fed by spatially restricted channels. The sampling was concentrated on the lobe areas, since flow rates in the channels are likely to have been higher than those in the lobes that they fed and these high flow rates may have been able to transport large pieces of solidified lava from previous flow events. Although almost all of Borgarhraun is extremely fresh, rock with vesicles filled by soil or by hydrothermal minerals or where the olivines had been strongly discolored by oxidation was avoided during sampling. Hydrothermal alteration is present in a small area in the northernmost limb of the flow, and no samples were taken from this area. Samples were taken both from the surface of the flow and from inside fissures which are up to 10 m deep.

[5] The position of each sample was located using a Magellan GPS Satellite Navigator with a WGS84 datum; the RMS horizontal error in the position is  $\sim 30$  m. The sample positions are shown on Figure 1, along with the digitized flow margin, fissure positions and edges of channels that are visible on the aerial photographs. The features from the aerial photographs were digitized by first tracing each feature on every photograph and then merging the traced images using reference points common to the photographs. The digitized Cartesian coordinates were then converted into map coordinates using reference points where the position of a feature on the aerial photos could be recognized on the map. The RMS horizontal error in recovering reference point positions was  $\sim 100$  m. The errors in this conversion do not affect the spatial variability results shown in section 7, since those results are based only on GPS measurements.

[6] Variability in crystal content and vesicularity is visible on the outcrop scale in Borgarhraun. Where the structure of the flow lobes is visible in fissures, the uppermost 1–2 m of the flow is composed of vesicular (20–30% vesicles) platy basalt, while the lower parts of the flow are massive and vesicle poor ( $\sim 5\%$ ), save for rare vesicle pipes and sheets with diameters of 1–10 cm. Pegmatitic or rhyolitic segregation structures were not observed. Variation in crystal and vesicle content and groundmass texture is also clearly visible on the hand-specimen and thin-section scale. Almost all hand specimens contain large olivine crystals (up to 8 mm in diameter), commonly accompanied by dark green chrome-diopside and plagioclase. Thin sections of 5 cm  $\times$  2 cm size were cut from the edge of all 77 of the samples. The crystal content of 23 of the thin sections was estimated by point counting with  $\sim 1000$  points per section. This method does not produce reliable estimates of the crystal content when the heterogeneity of the samples observed in hand specimen is large or when the phenocryst content is small. The crystal content in the thin sections varied from 2% to 20% (corrected for vesicle counts), with an average of 7.9%(87%) olivine, 0.7%(7%) plagioclase, 0.6%(6%) clinopyroxene, and 0.04%(0.4%) chrome-spinel. The values in parentheses show the percentage of the mineral as a total of the crystal content of the magma.

The individual modes are given in Table B1 of the electronic supplement<sup>1</sup>.

[7] Each sample shows a range of crystal sizes in both the groundmass and phenocryst populations. Olivine phenocryst sizes within a single thin section commonly vary from  $>5$  mm to  $<0.2$  mm. Olivine is most commonly euhedral but blocky and skeletal olivines are also present. The olivines are in general extremely fresh, but thin sections of six of the samples contain olivines where hematite and/or magnetite growth has taken place on margins or cracks. Plagioclase phenocrysts show a similar range in size to the olivines and while larger plagioclases are tabular or lath-shaped in thin section, smaller plagioclases are typically acicular. Again, the chrome-diopsides show a similar range in sizes and their morphologies are subhedral to rounded. Several of the chrome-diopsides show signs of resorption at their margins, and this feature is probably caused by their transit from depths where they are in equilibrium with their host melt to the surface, where the clinopyroxene stability field is small [MacLennan *et al.*, 2001]. Small crystals ( $<1$  mm) of chrome spinel are present in many of the samples. They show euhedral or hopper shapes when they are hosted by the groundmass and are rounded when they occur as inclusions in olivine. Melt inclusions are found in all of the phenocryst types, and occur most frequently in olivine and chromite. The olivine-hosted melt inclusions range in size from  $>200$   $\mu\text{m}$  to  $<10$   $\mu\text{m}$ . While the largest inclusions are typically rounded, triangular and negative crystal shaped inclusions are also present. All of the observed olivine-hosted melt inclusions appear to be primary because their positioning is not controlled by the presence of fractures and they are randomly arrayed within the host crystals [Roedder, 1984]. The inclusions are either mixed glass/microcrystalline or crystalline with a feathery texture. Shrinkage bubbles appear to be absent from the melt inclusions but may be hidden by crystal growth in the inclusions. The groundmass of the samples is dominated by plagioclase and pyroxene with smaller proportions of olivine and oxides. In the coarsest parts of the flow, which tend to be in the massive interior, doleritic textures with acicular plagioclases up to 100  $\mu\text{m}$  in length are present. In finer-grained samples the groundmass can be cryptocrystalline. Vesicles present within the hand specimens and thin sections of the analyzed samples are empty and segregation vesicles and veins were not observed.

### 3. Analytical Techniques

[8] The samples were split with a diamond saw and thin sections were taken from the edge of the part of the sample that was to be geochemically analyzed. At this stage, seven of the samples were discarded due to the presence of soil filling vesicles. The samples were split into two sets, one that is kept at the University of Cambridge and the other at the Nordic Volcanological Institute. The sawn samples were cleaned with distilled water and dried for 24 hours. Approx-

<sup>1</sup>Supporting data Tables B1–B3 are available via Web browser or via Anonymous FTP from <ftp://kosmos.agu.org>, directory "apend" (Username = "anonymous", Password = "guest"); subdirectories in the ftp site are arranged by paper number. Information on searching and submitting electronic supplements is found at [http://www.agu.org/pubs/esupp\\_about.html](http://www.agu.org/pubs/esupp_about.html).

**Table 1.** Variability in Borgarhraun Whole Rock Samples<sup>a</sup>

	$\bar{x}$	$\sigma_o$	$\sigma_r$	$\sigma_t$	$\sigma_r/\sigma_r$	$P, \%$	$V, \%$
SiO <sub>2</sub>	48.42	0.25	0.07	0.24	3.43	0.14	0.50
TiO <sub>2</sub>	0.68	0.04	0.00	0.04	8.97	0.60	5.88
Al <sub>2</sub> O <sub>3</sub>	14.48	0.37	0.03	0.37	12.33	0.21	2.55
FeO	8.22	0.17	0.01	0.16	16.00	0.12	1.95
MnO	0.17	0.00	0.00	—	—	1.90	—
MgO	11.78	0.61	0.02	0.61	30.48	0.17	5.18
CaO	12.83	0.20	0.02	0.20	9.95	0.16	1.56
Na <sub>2</sub> O	1.62	0.05	0.03	0.04	1.33	1.85	2.47
K <sub>2</sub> O	0.05	0.00	0.00	0.00	6.25	1.27	0.00
P <sub>2</sub> O <sub>5</sub>	0.05	0.00	0.00	0.00	3.05	1.87	0.00
La	1.68	0.11	0.08	0.08	1.03	4.70	4.76
Ce	4.39	0.29	0.10	0.27	2.60	2.36	6.15
Pr	0.70	0.05	0.02	0.04	2.22	2.86	5.71
Nd	3.71	0.26	0.10	0.24	2.44	2.69	6.47
Sm	1.41	0.11	0.03	0.10	2.96	2.48	7.09
Eu	0.55	0.04	0.02	0.03	1.57	3.62	5.45
Gd	1.87	0.10	0.05	0.09	1.83	2.62	4.81
Tb	0.35	0.02	0.01	0.02	2.37	2.27	5.71
Dy	2.39	0.14	0.08	0.12	1.38	3.51	5.02
Ho	0.53	0.03	0.02	0.02	1.00	4.52	3.77
Er	1.55	0.10	0.07	0.08	1.11	4.38	5.16
Tm	0.24	0.02	0.01	0.01	1.31	4.56	4.17
Yb	1.52	0.09	0.03	0.08	2.40	2.23	5.26
Lu	0.24	0.02	0.01	0.01	1.03	4.56	4.17
Nb	1.62	0.22	0.18	0.13	0.71	11.03	8.02
Zr	30.75	1.58	0.36	1.54	4.32	1.16	5.01
Y	16.02	0.70	0.28	0.64	2.25	1.76	4.00
Sr	86.07	2.67	0.66	2.59	3.91	0.77	3.01
Rb	0.54	0.32	0.26	0.19	0.73	48.88	35.19
Zn	71.02	2.20	1.05	1.93	1.84	1.48	2.72
Cu	111.66	8.30	0.92	8.25	8.97	0.82	7.39
Ni	277.21	32.92	1.79	32.87	18.36	0.64	11.86
Cr	795.20	131.95	3.29	131.91	40.09	0.42	16.59
V	244.59	5.58	3.23	4.55	1.41	1.32	1.86
Ba	16.26	4.16	4.04	0.99	0.25	25.85	6.09
Sc	45.95	2.06	1.04	1.78	1.71	2.26	3.87
Zr/Y	1.92	0.06	0.03	0.05	1.58	1.66	2.69
u <sub>1</sub>	18.60	1.10	0.21	1.08	5.20	1.07	—
u <sub>2</sub>	0.45	0.43	0.23	0.36	1.58	51.11	—

<sup>a</sup>The average values are given by  $\bar{x}$  and the observed standard deviation is  $\sigma_o$ . The elements expressed as oxides are given in wt %, the remaining elements are given in ppm. These values are based on 70 whole rock samples. The precision estimate from repeat runs of samples is  $\sigma_r$ , the true standard deviation of the samples when corrected for noise is  $\sigma_t$ . The signal-to-noise ratio is given by  $\sigma_r/\sigma_t$ , the percentage precision,  $P$ , is  $100 \times \sigma_r/\bar{x}$ , the percentage variability compared to the mean value,  $V$ , is given by  $100 \times \sigma_o/\bar{x}$ . The first two principal components for the REEs are labeled u<sub>1</sub> and u<sub>2</sub>.

imately 100 g of each sample was crushed in a manganese steel jaw crusher and then powdered in an agate planetary ball mill for 30 min. This powdering process generated a visually homogeneous powder.

### 3.1. X-Ray Fluorescence Analysis

[9] The powdered samples were prepared for X-ray fluorescence (XRF) analysis at the University of Edinburgh, using the technique described by *Fitton et al.* [1998]. Two separate aliquots of powder were taken from each sample, one to prepare fusion discs for major and minor element analysis and another to prepare pressed powder pellets for trace element analysis. Fusion discs were made after mixing sample powder with lithium tetraborate flux which provides a low atomic number matrix into which the elements are dissolved. The samples were dried for at least 4 hours in an oven at 110°C, and then a nominal but precisely weighed 1 g of sample was ignited at 1100°C to allow calculation of the mass loss on ignition (LOI). Then the samples were mixed with the flux, fused, poured and cast into discs. Trace

element concentrations were determined on pressed powder samples which contained 6 g of sample and four drops of a 2% aqueous solution of polyvinyl alcohol. The discs were run on a Philips PW 1480 automatic XRF spectrometer with a Rh-anode X-ray tube and the analytical conditions are used are those given by *Fitton et al.* [1998]. The spectrometer was calibrated with USGS and CRPG standards using the values given by *Jochum et al.* [1990] for Nb and Zr and *Govindaraju* [1994] for the other elements. The LOI was negative (about -0.5%) for almost all of the samples and this mass gain is due to the oxidation of iron. Precision and accuracy were estimated by 3 repeat runs of USGS standards BIR-1 and BHVO-1 and 10 repeat runs of the prepared powder pellet and fusion disc for sample FH9801. The precision estimates given in Table 1 are only based on the repeats of FH9801 and are calculated using  $\sigma_r = \sqrt{\sum(\Delta x)^2/(n-1)}$  where  $\Delta x$  is the difference between a given repeat measurement of a sample and the mean of the repeat measurements of that sample and  $n$  is the total number of repeats. Details of XRF measurements made on 10 Borgarhraun samples using a high precision machine are given in Appendix A.

### 3.2. Inductively Coupled Plasma Mass Spectrometry

[10] The samples were prepared for ICP-MS analysis by HF dissolution at the University of Cambridge. The powders were dried overnight and  $0.5000 \pm 0.0003$  g of powder were weighed into clean teflon beakers. A few drops of millipore water were added to make a slurry, and then 6 mL of Aristar concentrated HF and 10 mL Aristar concentrated HNO<sub>3</sub> were poured with care into the beaker. The beakers were covered and the samples refluxed for 4 hours after which time the powder had been digested. Then the sample solutions were left to evaporate to near dryness. Then 5 mL Aristar concentrated HNO<sub>3</sub> were added to the residue, and the samples were refluxed for 2 hours under lids and then evaporated to near dryness. A further 5 mL HNO<sub>3</sub> was added, and the solutions were refluxed for 2 hours. These solutions were then transferred to 250 mL volumetric flasks, and the flasks were filled with millipore water. At this stage the samples were at 1:500 dilution. The flasks were then left to stand overnight on a hot plate, and the solutions were transferred to 60 mL nalgene bottles which were sealed. Procedural blank solutions were prepared along with each batch of samples, and each reference standard was prepared with more than one batch. The sample solutions were analyzed for rare earth elements (REEs) on the research machine at the NERC ICP-MS facility, Centre for Analytical Research in the Environment at Silwood Park, Ascot, United Kingdom. The sample solutions were diluted by another factor of 10 to 1:5000 to reduce suppression. Only the mass range from <sup>139</sup>La to <sup>172</sup>Lu was scanned, and calibration solutions at low concentrations were used. The calibration solutions for the Borgarhraun samples were prepared to reflect natural compositions and had La/Ce = 0.5 and La/Lu = 2. These calibration solutions were prepared with La concentrations of 2, 5, and 10 ppb. Throughout the analyses, the lowest concentration calibration solution was run as a drift monitor every five samples. The procedural blanks were under 1% of the lowest sample concentrations measured, and all the measurements were over 200 times the detection limits. The ICP-MS machine was washed with dilute nitric acid

between each sample run. Analyses of reference materials were interspersed with the unknowns. The precision estimates given in Table 1 are based on 12 repeat runs of multiple preparations of BIR-1 (6 repeats) and FH9801 (6 repeats). The compositions of the whole rock samples are given in Table B1 of the electronic supplement.

### 3.3. Secondary Ionization Mass Spectrometry

[11] For the melt inclusion study, nine Borgarhraun samples were selected and hand-crushed with a steel pestle and mortar. Olivine crystals were hand-picked from the crush. The melt inclusions were rehomogenized by heating in a vertical 1 atm quench furnace held at 1240°C and an oxygen fugacity one log unit beneath the quartz-fayalite-magnetite buffer. The samples were held at these conditions for ~20 min in a Pt crucible and were quenched rapidly by dropping the crucible into water. Next, the crystals were set in epoxy and the melt inclusions were exposed by grinding and polishing with Buehler Alpha diamond and alumina micro-polish. Inspection of the melt inclusions after heating showed that they were glassy, devoid of bubbles and had retained their original shape. The Cameca IMS 3f ion probe at Woods Hole Oceanographic Institute was used to analyze 43 melt inclusions from 32 olivines from nine samples for selected REEs and trace elements. The analyses were carried out during February 1999. The analytical procedure is described in detail elsewhere [Shimizu and Hart, 1982; Shimizu, 1998]. The polished samples were gold coated and then bombarded by a beam of negatively charged oxygen ions ( $O^-$ ) with a net voltage of ~12.5 kV. Near-circular beams with diameters of 20  $\mu\text{m}$  and 5  $\mu\text{m}$  were used for REE and trace element analyses respectively. Only melt inclusions >30  $\mu\text{m}$  diameter were analyzed. Molecular ion interferences were suppressed using the energy filtering technique [Shimizu and Hart, 1982], so the secondary accelerating voltage was offset by 90 V for REE analysis and 60 V for other elements. Element abundances were calculated by converting secondary ion intensity (ratioed to  $^{30}\text{Si}$ ) with empirical relationships between intensity and concentration; the specific relationship used here was calculated from an enlarged version of the database developed by Johnson *et al.* [1990] for basalt glasses. The precision and accuracy were estimated using repeat analyses of a single melt inclusion (FH9806-2.1) and a Hawaiian basalt glass internal standard (KL2). The 5 runs of FH9806-2.1 gave a precision of 10–20% ( $100\sigma/\bar{x}$ ) for the REEs and KL2, which has much higher REE concentrations than the Borgarhraun sample, gave a precision of 2–5% for the middle and heavy REEs and 5–10% for La and Ce. The accuracy estimates for KL2 are similar to those of the precision. Shimizu [1998] found similar uncertainties for the glass standard and showed that the analytical uncertainties originate mainly in counting statistics. The precision estimate for the Borgarhraun melt inclusions given in Table 2 was calculated by combining the repeats of FH9806-2.1 with repeat measurements of 19 samples of similar olivine-hosted melt inclusions from Theistareykir on the same machine described by Slater *et al.* [2001].

### 3.4. Electron Microprobe

[12] The concentrations of major and selected minor elements in the crystals and melt inclusions from Borgarhraun

**Table 2.** Variability in Borgarhraun Melt Inclusions<sup>a</sup>

	$\bar{x}$	$\sigma_o$	$\sigma_r$	$\sigma_t$	$\sigma_t/\sigma_r$	$P, \%$	$V, \%$
La	1.12	0.66	0.25	0.61	2.48	22.03	54.46
Ce	3.00	1.46	0.41	1.40	3.41	13.69	46.67
Nd	2.70	0.93	0.63	0.69	1.09	23.28	25.55
Sm	1.17	0.28	0.19	0.20	1.06	16.43	17.09
Eu	0.50	0.15	0.09	0.12	1.33	18.00	24.00
Dy	2.10	0.49	0.23	0.43	1.84	11.12	20.48
Er	1.51	0.30	0.25	0.17	0.70	16.28	11.26
Yb	1.54	0.29	0.17	0.23	1.36	11.15	14.94
$u_1$	3.77	4.08	1.01	3.95	3.91	26.80	–
$u_2$	2.54	1.66	0.73	1.49	2.05	28.61	–

<sup>a</sup>Columns are the same as those for Table 1. The values are based on 43 melt inclusion compositions. The principal components for the REEs are represented by  $u_n$ , the principal components are given in Table 4.

raun were determined using a Cameca SX50 electron microprobe at the University of Cambridge. A review of electron microprobe methods is given by Reed [1996]. The olivines hosting the melt inclusions were polished and carbon coated. The concentrations for the major elements were determined in energy dispersive (ED) mode with a count time of 60 s. Quantitative ED analysis uses the ZAF4 least squares profile fitting technique and stored elementary peak profiles from standards such as periclase (Mg), pure iron (Fe), wollastonite (Ca, Si) and corundum (Al). The probe was calibrated with these standards before the start of each session. The accuracy and precision for major elements present at >5 wt % oxide is ~1% ( $1\sigma$  relative precision) for ED analysis; the precision can be calculated from the counting statistics as described by Reed [1996]. The Ni and Ca contents of a selected number of olivines were also measured using wavelength dispersive spectroscopy (WDS). During the WDS analysis a count time of 60 s was used on the peak and 20 s on the background. For melt inclusion analysis the beam width was 5  $\mu\text{m}$  with a current of 12 nA and acceleration voltage of 20 kV. For host olivine analyses a current of 20 nA was used. Samples with totals outwith the range 99–101% were discarded. The compositions of the melt inclusions and their olivine hosts are given in Table B2 of the electronic supplement. Elements whose peak heights were less than three standard deviations of the background count are not given in Table B2.

## 4. Compositional Variability

[13] Variability is present in the sample set for all of the elements that were measured. However, both random and systematic errors affect the measurements and part of the variability is due to these measurement errors. While random errors may have an important effect on the measured sample variability, systematic errors will be unimportant. The standard random error,  $\sigma_r$ , of each element was estimated with repeat analyses, and removed from the observed standard deviation of the sample set,  $\sigma_o$ , to give an estimate of the true standard deviation,  $\sigma_t^2 = \sigma_o^2 - \sigma_r^2$ , and the signal-to-noise ratio,  $\sigma_t/\sigma_r$  [Slater *et al.*, 2001]. The magnitude of  $\sigma_o$  is greater than that of  $\sigma_r$  for all of the measured elements apart from Mn. However,  $\sigma_r$  is an estimate of the true analytical error,  $\sigma_R$ , based on a limited number of repeat measurements (e.g., 10 runs of FH9801 for the XRF precision) and there is uncertainty in this estimate. If  $\sigma_R > \sigma_o$ , then there is no true variability in the

sample set. The  $\chi^2$  distribution can be used to test the null hypothesis that  $\sigma_R \geq \sigma_o$  [e.g., *Hoel*, 1962; *Kreyszig*, 1993]. The alternative hypothesis is that  $\sigma_R < \sigma_o$ . The  $\chi^2$  distribution is tabulated in many standard textbooks [e.g., *Kreyszig*, 1993, Table A11, p. A106]. If  $n$  is the number of repeat measurements used to determine  $\sigma_r$ , then the number of degrees of freedom,  $f$ , is given by  $n - 1$ . For  $f = 9$  and a significance level of  $\alpha = 0.01$  the critical value,  $c$ , is 2.09. For a test with  $\alpha = 0.01$  the probability of a type I error, that is rejecting the null hypothesis when it is true, is 0.01. The random variable  $Y = fS^2/\sigma^2$  has a  $\chi^2$  distribution where  $S^2$  is the sample variance and  $\sigma^2$  is the population variance [e.g., *Kreyszig*, 1993, p. 1240]. For this test the population variance is the true analytical variance (i.e.  $\sigma^2 = \sigma_R^2$ ), and the calculated value of  $S^2$  is compared with the observed variance from the repeat measurements,  $\sigma_r^2$ . If the null hypothesis is true, then  $\sigma_R^2 \geq \sigma_o^2$ . If  $\sigma^2 = \sigma_o^2$  and  $Y = c$ , then rearrangement of the expression for  $Y$  gives  $S^2 = c\sigma_o^2/f$ . If  $\sigma_r^2 \geq S^2$ , then the null hypothesis is accepted. By using  $\sigma_o^2 = \sigma_t^2 + \sigma_r^2$  and rearranging the inequality it can be shown that the null hypothesis of no natural variability is accepted at the 0.01 significance level if the signal to noise ratio,  $\sigma_t/\sigma_r$ , is  $< 1.81$ . The same null hypothesis can be accepted at  $\alpha = 0.05$  if  $\sigma_t/\sigma_r \leq 1.3$ . Therefore the conclusions reached in the following few sections are, wherever possible, based on elements with  $\sigma_t/\sigma_r > 2$ . Furthermore, the conclusions do not depend on elements which are poorly determined by ICP-MS (e.g., Eu, Gd) or XRF (e.g., Rb, Ba, Nb).

[14] The values of  $\sigma_t/\sigma_r$  are listed in Table 1 for all of the measured elements. For 20 of the 36 elements measured the signal to noise ratio is greater than 2, including incompatible trace elements (e.g., Ce, Zr), compatible trace elements (e.g., Ni, Cr) and major elements (e.g., MgO, FeO). The signal to noise ratio for Zr/Y is 1.58 so it is likely that there is true variability in ratios of incompatible trace elements in the Borgarhraun samples. Further evidence that there is true variation in the Borgarhraun whole rock sample compositions comes from a number of sources. The correlation coefficients of the elements are shown in Table B3 of the electronic supplement. Pairs of elements which display similar behavior in basaltic systems but were measured in different aliquots of sample and/or on different machines show high correlation coefficients,  $r$ . For example, MgO (fusion disc, XRF) and Ni (powder pellet, XRF), have  $r = 0.89$ , TiO<sub>2</sub> (fusion disc, XRF) and Zr (powder pellet, XRF), have  $r = 0.94$  and TiO<sub>2</sub> and Nd (ICP-MS) have  $r = 0.69$ . Mg and Ni are both highly compatible in olivine, while Ti, Zr, and Nd are all incompatible during mantle melting and the early stages of basalt crystallization. If the measured concentrations were controlled by measurement errors or by heterogeneous contamination during XRF or ICP-MS sample preparation or by incomplete mixing of the sample powders, then all of the correlations between elements measured on different sample aliquots or with different methods would be close to zero. Furthermore, in section 7 it is shown that the concentrations of moderately incompatible elements (e.g., Zr, Ti, Nd) have a highly nonrandom spatial distribution within Borgarhraun. It is extremely unlikely that such spatial variations would be observed if the measured compositional variation in these elements was caused by analytical noise, by contamination during preparation or by incomplete mixing of sample powders. The

variability caused by powder heterogeneity within single samples is quantified in Appendix A. Incorporation of the estimates of this powder heterogeneity into the  $\sigma_r$  estimates for trace elements measured by XRF makes little difference to the estimates of  $\sigma_r$  and, for example, the  $\sigma_r$  of Zr is reduced from 1.54 to 1.53 ppm and that of Ni from 32.87 to 32.77 ppm when powder heterogeneity is included. Finally, the results of high precision XRF measurements on 10 samples described in Appendix A also show true variability with  $\sigma_t/\sigma_r > 5$  for both incompatible (Zr, Y, Sr) and compatible (Ni, Cr) trace elements.

[15] The variability in the REE concentrations in the whole rock samples and melt inclusions is shown on Figure 2. The REE concentrations in the melt inclusions are also variable, with signal to noise ratios of up to 3.4. The range in REE variability observed in the present set of Borgarhraun melt inclusions is similar to that found by *Slater et al.* [2001] who analyzed olivine-hosted melt inclusions from five primitive flows from Theistareykir, including Borgarhraun.

[16] Principal component analysis is a powerful method which can be used to handle multivariate data such as geochemical measurements on multiple samples [see *Reyment and Jöreskog*, 1993, and references therein]. Application of principal component analysis to problems in igneous petrology has been described by several authors [*LeMaitre*, 1982; *Albarède*, 1995], and some of the details of the principal component analysis method used in this paper have been given by *McKenzie and O'Nions* [1998] and *Slater et al.* [2001]. The main advantage of principal component analysis is that it can be used to reduce the number of variables required to describe the greater part of the variability within a multivariate data set. If the concentration of  $N$  elements is measured in every sample from a set of  $M$  rock samples, then the data set can be displayed as an  $M \times N$  matrix. If the data are plotted with the elements as the orthogonal axes, then the data set consists of a cloud of  $M$  points in an  $N$ -dimensional space. By rigid rotation of the axes it is possible to describe the data in terms of a new set of  $N$  independent variables called principal components which can be sorted into order of decreasing variability of the data in the relevant direction. The principal components correspond to the eigenvectors,  $\mathbf{u}_n$ , of the covariance matrix of the data, which can be found using methods described by *Reyment and Jöreskog* [1993] or *Press et al.* [1992]. Each of the eigenvectors has an associated eigenvalue,  $\lambda_n$ . The larger the value of  $\lambda_n$ , the greater the amount of variability described by the principal component. In plots of principal components such as those shown in this paper, mixing lines are straight and obey the lever rule. In this study, one set of principal components is calculated from the REE data alone and others are calculated from the major element concentrations (Si, Al, Fe, Mg, Ca). For the major element and REE data, the first two principal components account for  $\sim 90\%$  of the observed variability. The  $\sigma_r$  values for the principal components were calculated by projecting the repeat measurements onto the principal components. The first principal components have high signal to noise ratios (as shown in Tables 1 and 2). These high signal to noise ratios are further evidence that there is true variability in both major and trace element concentrations in the samples from Borgarhraun. The principal components that were determined for the REEs and major elements are shown in Tables 3, 4, and 5.

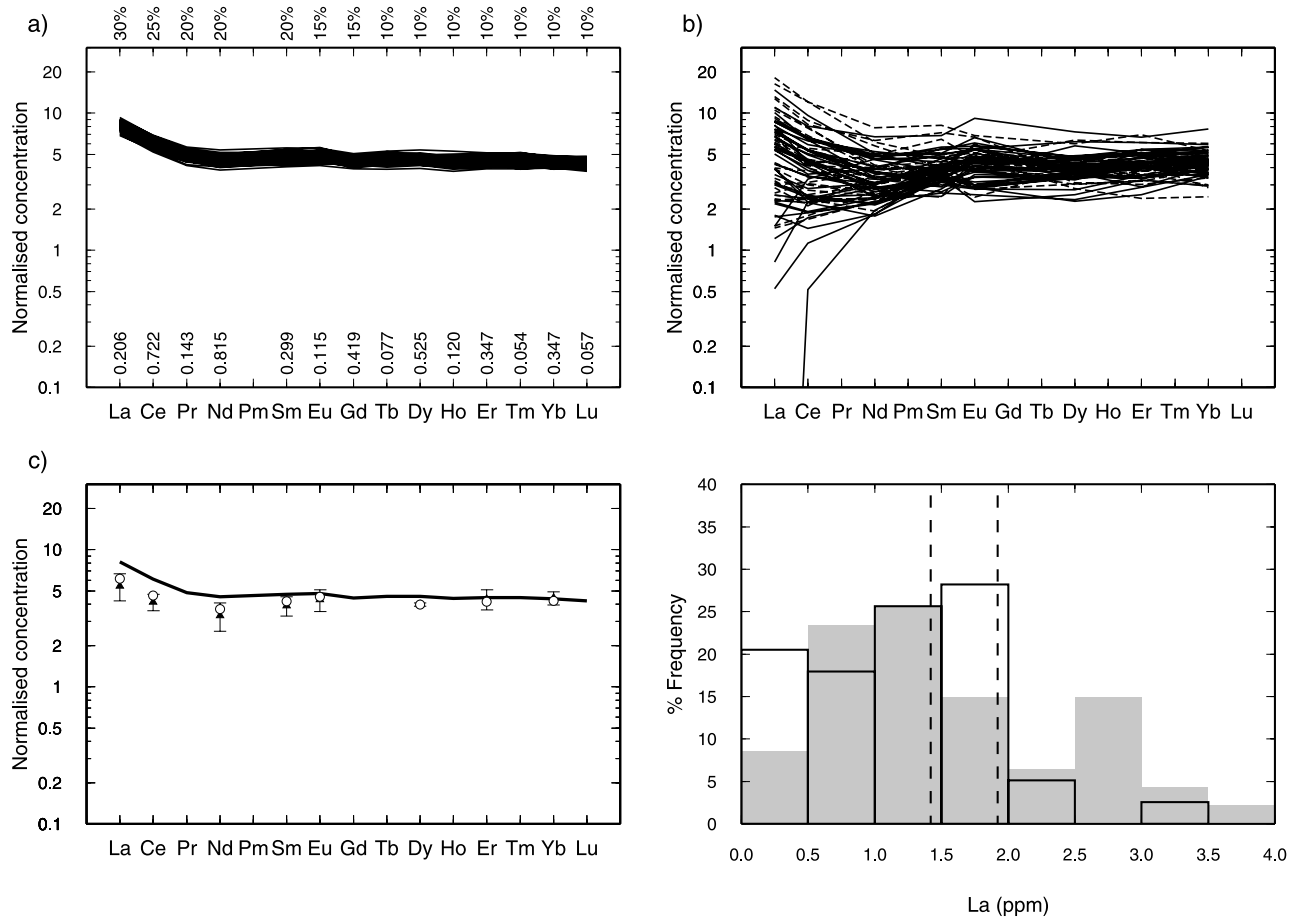


**Figure 2.** REE concentrations of whole rock and melt inclusion compositions from Borgarhraun. Concentrations normalized to the MORB source of *McKenzie and O’Nions* [1991] and plotted on a log scale. (a) Borgarhraun whole rock compositions. The numbers on the bottom axis show the concentrations of the elements in the MORB source used for normalization, and the numbers on the top axis show the estimated errors in this source concentration. (b) Olivine hosted melt compositions. The solid lines show samples from this study, and the dashed lines show the different set of Borgarhraun samples from *Slater et al.* [2001]. (c) Comparison of average melt inclusion and whole rock compositions. Solid line shows average whole rock composition, solid triangles show average olivine hosted melt inclusion composition from this study, and open circles show the average from *Slater et al.* [2001]. The error bars show the  $\pm 1\sigma$  precision estimate for the SIMS measurements. (d) Histogram of La concentrations in Borgarhraun melt inclusions. The boxes marked with a solid line show samples from this study, and shaded boxes show samples from *Slater et al.* [2001]. The dashed lines mark the extremes of the Borgarhraun whole rock compositions.

[17] In the principal component method described by *McKenzie and O’Nions* [1998] the measured elemental concentrations are divided by a mantle composition before calculation of the covariance matrix. This process is referred to as normalization in this paper. The principal components are dependent on the normalization used and the effect of changing the normalization for the major elements is shown in section 5.2. However, the cross-correlation coefficients are independent of the normalization. The magnitudes of the correlation coefficients between incompatible trace elements (e.g La, Zr) and compatible major elements (e.g., Ca, Mg) are small, and Figure 3a shows the poor correlation between MgO and Nd. There is also a poor correlation between the principal components for REEs and major elements (Figure 3b). This poor

**Table 3.** Whole Rock REE Principal Components<sup>a</sup>

$\sqrt{\lambda_n}$	La	Ce	Pr	Nd	Sm	Eu	Gd
$\mathbf{u}_1$	1.100	0.39	0.34	0.29	0.28	0.31	0.18
$\mathbf{u}_2$	0.429	-0.77	-0.21	-0.09	-0.07	0.17	0.04
$\mathbf{u}_3$	0.174	0.33	-0.18	-0.22	-0.28	0.05	-0.53
$\sqrt{\lambda_n}$	Tb	Dy	Ho	Er	Tm	Yb	Lu
$\mathbf{u}_1$	1.10	0.22	0.22	0.24	0.24	0.26	0.21
$\mathbf{u}_2$	0.429	0.12	0.18	0.17	0.22	0.30	0.22
$\mathbf{u}_3$	0.174	0.04	-0.24	-0.13	0.07	0.41	0.34

<sup>a</sup>Principal components for REEs in whole rock samples. The first column shows the square root of the eigenvalues ( $\lambda_n$ ) for the eigenvectors  $\mathbf{u}_n$ . The eigenvectors are given in rows and are ordered by the magnitude of the eigenvalues. Only the first three principal components are shown. The eigenvectors were determined using the method of *Slater et al.* [2001].

**Table 4.** Melt Inclusion REE Principal Components

	$\sqrt{\lambda_i}$	La	Ce	Nd	Sm	Eu	Dy	Er	Yb
<b>u<sub>1</sub></b>	4.08	0.77	0.49	0.24	0.13	0.24	0.11	0.11	0.09
<b>u<sub>2</sub></b>	1.66	-0.35	-0.12	0.21	0.35	0.46	0.45	0.36	0.40
<b>u<sub>3</sub></b>	0.775	0.31	-0.24	-0.57	-0.38	-0.17	0.33	0.36	0.34

correlation shows that the processes that control major element variation are decoupled from those that cause variation in trace element abundances. The variability of incompatible element absolute abundances and ratios in both the whole rock samples and the melt inclusions are not likely to be the result of fractional crystallization (or crystal accumulation), because small amounts of crystallization cause uniform increases of incompatible element concentrations and do not change incompatible element ratios. Also, if fractional crystallization controlled the variation in REE concentrations, indicators of degree of crystallization (such as MgO content) would correlate with incompatible element concentrations. It is probable that part of the variation in REE concentrations observed in Borgarhraun samples is a result of melting, since fractionation of incompatible elements can occur at the low porosities expected to exist in the melting region under mid-ocean ridges.

## 5. Causes of Compositional Variability

### 5.1. Rare Earth Elements

#### 5.1.1. Mantle Melting

[18] The Borgarhraun lava flow makes up <1% of the total eruptive output of the Theistareykir system during the last 100 kyr, so its mean composition need not be representative of the mantle melting under Theistareykir. The range of magma compositions that can be produced by fractional melting of a single mantle source is controlled by the depth and extent of the melting. Both the average REE composition of Theistareykir lava and the crustal thickness of  $20.5 \pm 2.5$  km observed under the southern part of the Theistareykir system [Staples *et al.*, 1997] can be produced by a model where melting starts in the garnet stability field and reaches a melt fraction of  $\sim 0.26$  at the base of the crust [Slater *et al.*, 2001]. This melt fraction against depth relationship is shown in Figure 4a. The composition of the instantaneous fractional melts generated at any given depth in the model can be calculated by tracking the evolution of the residual mantle composition as it moves through the melting region [White *et al.*, 1992]. Figure 4b shows the compositions of the whole rock samples and the instantaneous fractional melts projected onto the plane of the first two principal components of the melt inclusion REEs (Table 4). The range of compositions of the predicted instantaneous fractional melts is much greater than that of the whole rock samples, and incomplete mixing of these fractional melts can match the compositions of the samples. The variability in melt inclusion compositions is larger than that of the whole rock samples, and can also be produced by mixing of fractional melt compositions, as shown in Figure 4e. Fractional melt compositions from shallower than 60 km are not required to produce the variability in the melt inclusions.

#### 5.1.2. Other Causes of Variability

[19] While the range of compositions of instantaneous fractional melts produced by melting of a single mantle

source is larger than that observed in either the Borgarhraun whole rock samples or melt inclusions, part of the observed variability is likely to be caused by variability in the composition of mantle that is entering the melting region [Stracke *et al.*, 2002]. However, the discussion of melt mixing and spatial variability presented in sections 6 and 7 holds regardless of the cause of compositional variation in the mantle melts.

[20] Boundary layer processes that occur during crystal growth can generate zones of high concentrations of incompatible elements around the growing crystal [Albarède and Bottinga, 1972; Lasaga, 1981]. If the enriched melt in the boundary layer becomes trapped in melt inclusions in the growing crystals, then the compositions of the melt inclusions will not be the same as that of the melt outside the boundary layer. A study of primary melt inclusions in olivine crystals has shown that melt inclusions <25  $\mu\text{m}$  in diameter had compositions different to that of the bulk melt outside the olivine boundary layer [Anderson, 1974]. However, a number of lines of argument show that it is unlikely that the REE compositional variation in the Borgarhraun melt inclusions is caused by boundary layer processes. The first is that no relationship between inclusion size or shape and the composition of the inclusions was observed in this study or that of Slater *et al.* [2001]. Inclusions with similar diameters often have very different compositions and, for example, inclusion 34-7.1 is rounded with a diameter of  $\sim 60 \mu\text{m}$  and a La content of 0.47 ppm, while inclusion 64-4.1 is rounded with a diameter of  $\sim 70 \mu\text{m}$  and a La content of 3.04 ppm. Another important observation is that many of the inclusions have La contents that are lower than those of any of the samples from primitive Theistareykir flows reported here and by Slater *et al.* [2001]. The boundary layer processes described above are likely to only cause increases in the La concentration of the melt because La is an incompatible element in olivine.

[21] The concentration of an element in the boundary layer is influenced by the rate of crystal growth,  $V$ , the thickness of the boundary layer,  $\delta$ , and the diffusion rate of the element in the melt,  $D$ . The maximum concentration of an incompatible element occurs at the interface with the crystal, and Lasaga [1981] showed that the concentration,  $C_i$ , of a perfectly incompatible element at the crystal-melt interface is given by  $C_i = C_0 \exp(V\delta/D)$  where  $C_0$  is the

**Table 5.** Major Element Principal Components<sup>a</sup>

	$\sqrt{\lambda_i}$	SiO <sub>2</sub>	Al <sub>2</sub> O <sub>3</sub>	FeO	MgO	CaO
<i>Depleted Mantle Source Normalized</i>						
Norm		45.64	2.70	8.02	40.75	2.40
<b>u<sub>1</sub></b>	0.155	0.026	0.881	-0.071	-0.082	0.461
<b>u<sub>2</sub></b>	0.051	0.012	-0.470	-0.141	-0.025	0.871
<b>u<sub>3</sub></b>	0.017	0.012	-0.025	0.927	-0.353	0.127
<i>Sample Average Normalized</i>						
Norm		48.42	14.48	8.22	11.78	12.83
<b>u<sub>1</sub></b>	0.0581	0.053	0.395	-0.108	-0.883	0.225
<b>u<sub>2</sub></b>	0.0222	0.071	0.317	-0.849	0.318	0.268
<b>u<sub>3</sub></b>	0.0117	-0.105	-0.836	-0.294	-0.248	0.377

<sup>a</sup>Borgarhraun whole rock principal components for major elements. The compositions of the normalizing materials are given in wt % of the oxide, with all Fe as FeO and are marked Norm. Rows and columns are labeled in the same way as Table 3. Only the first three principal components are shown.

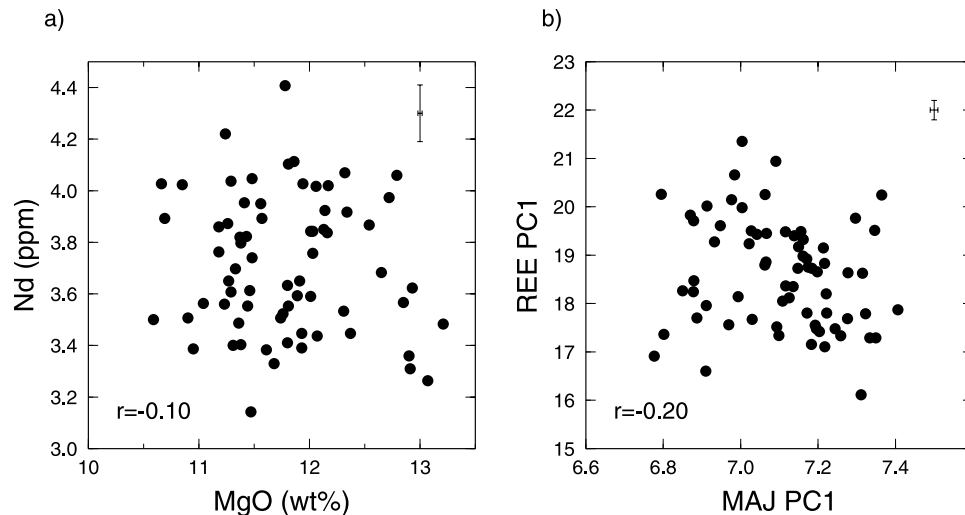


**Figure 3.** Borgarhraun whole rock samples. The error bars at the top right show the  $\pm 1\sigma$  precision estimates from repeat measurements. The correlation coefficient ( $r$ ) is shown in the bottom left corner. (a) Nd plotted against MgO content. (b) REEPC1, the first principal component for the REEs (Table 3), and MAJPC1, the first principal component for the major elements (Table 5).

concentration in the melt away from the growing crystal. Although the values of  $V$ ,  $D$  and  $\delta$  are not well known, a maximum estimate of  $C_l$  can be obtained by using low values of  $D$  for REEs in basaltic compositions, high rates of crystal growth rate in natural systems and large values of  $\delta$ . If  $D = 1.31 \times 10^{-11} \text{ m}^2 \text{ s}^{-1}$  [LaTourrette *et al.*, 1996] and  $V = 1.0 \times 10^{-11} \text{ m s}^{-1}$  [Kirkpatrick, 1977], then the concentration ratio  $C_l/C_0 \approx \exp\delta$ . If  $\delta < 10^{-4} \text{ m}$ , as suggested by Lasaga [1981], then the concentration of the element in the boundary layer will be indistinguishable from that in the melt away from the boundary layer.

[22] Several studies have shown that the REE concentration of whole rock samples of basaltic lava flows can be influenced by redistribution of incompatible elements which occurs during the final stages of crystallization of the flow [Rogan *et al.*, 1996; Goff, 1996; Caroff *et al.*, 2000]. This redistribution is commonly associated with the presence of vesicle pipes, filled segregation vesicles, segregation veins of rhyolitic or pegmatitic material and widespread alteration of olivines to iddingsite. Any segregation of late stage melts rich in incompatible elements that occurs in veins will generate compositional variation on a length scale of centimeters to meters. It is likely that this form of segregation does not have an important control on the composition of the whole rock samples from Borgarhraun both because there is a general lack of segregation features observed on outcrops, hand specimens and thin sections and because kilometer-scale variations in incompatible element concentrations are present in the flow (see section 7).

## 5.2. Major Elements

[23] Although the depth and degree of melting influences the major element composition of mantle melts, the principal control on the major element composition of mid-ocean ridge basalts is crystallization at low pressures [Grove *et al.*, 1992]. The major element compositional variation of the Borgarhraun whole rock samples is shown in Figure 5. Any curve that passes through all of the sample points (within

error) must possess numerous maxima and minima within the range of Borgarhraun MgO compositions. The presence of maxima and minima in liquid line of descent models is typically controlled by the addition of new phases to the crystallizing assemblage as solidification proceeds [Grove *et al.*, 1992; Langmuir *et al.*, 1992]. Only four phenocryst phases are observed in Borgarhraun samples, so it is extremely unlikely that the observed compositional variation tracks a liquid line of descent of a single parental melt composition. Therefore at least two different processes are required to explain the major element variability of the whole rock samples. Principal component analysis was used to find the composition of material that has to be added/removed to produce the observed trends in the major element contents of the samples [MacLennan *et al.*, 2001].

[24] The choice of the composition used to normalize the whole rock concentrations can have an important effect on the principal component analysis. For REE concentrations in mantle melts, which are directly proportional to the mantle source concentration, it is reasonable to use an estimated mantle source composition for normalization. However, in the case of major element concentrations, the link between the mantle source composition and the variability in liquid composition is obscured by fractional crystallization. For this reason, two different normalizations were used to determine the principal components for the major elements; one where the concentrations were normalized to the depleted mantle source and another where the concentrations were normalized to the average composition of the whole rock samples.

[25] The principal components found for the different normalizations are shown in Table 5. The first two principal components describe more than 90% of the variance for both normalizations. The eigenvalues of the principal components are controlled by the concentrations used for normalization. The components of the first principal component are similar for both of the normalizations, in that  $\text{Al} > \text{Ca} > \text{Si} > \text{O} > \text{Fe} > \text{Mg}$ . The high MgO content of the

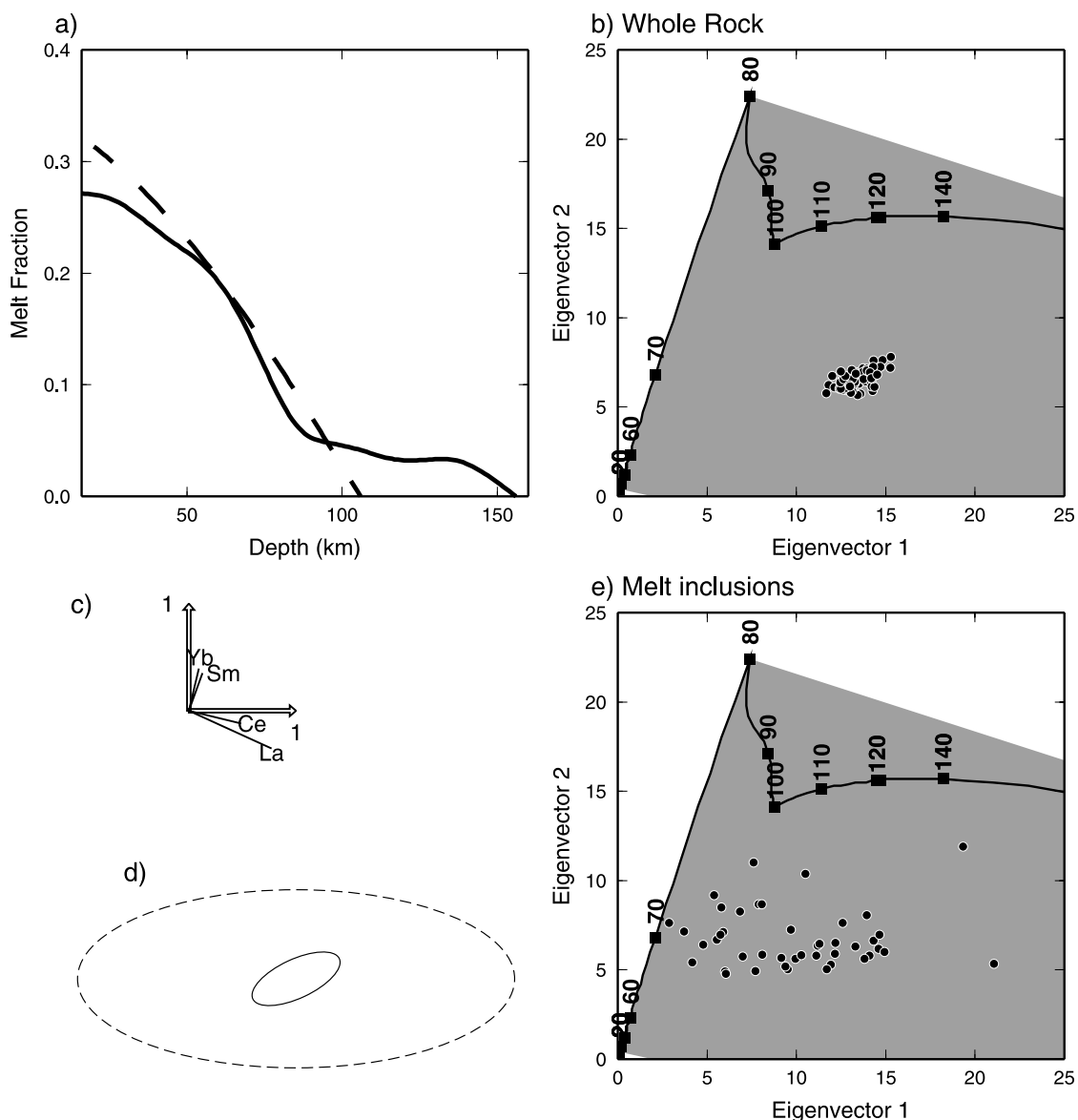


**Figure 4.** (a) Solid line showing a melting model which fits the average REE composition of Theistareykir lava [Slater *et al.*, 2001; MacleNNan *et al.*, 2001] and dashed line showing the melt fraction against depth relationship for mantle with a potential temperature of 1480°C calculated using the parameterization of Watson and McKenzie [1991]. Garnet is stable at depths >80 km, and spinel is stable at depths <100 km. (b) Small shaded circles with white outlines showing the projection of the whole rock sample compositions onto the eigenvectors for the melt inclusion REEs given in Table 4. The compositions of the instantaneous fractional melts produced by the Theistareykir melting model in Figure 4a are shown by the solid line. The extreme compositions produced during the initial stages of melting are not plotted. The first melt has a first eigenvector score of 181 and a second eigenvector score of -38. The numbered squares show the depth (in km) at which the fractional melt is produced. The kinks in the fractional melt path are caused by the spinel-garnet transition. The range of melt compositions that can be produced by mixing of instantaneous fractional melts is shaded. (c) Projection of selected elements onto the principal components used in Figure 4b. Unit vectors parallel to the principal components are shown by arrows. (d) Relative orientation and magnitude of principal components for melt inclusion and whole rock compositions. The lengths of the principal axes of the dashed ellipse are proportional to the standard deviation  $\sqrt{\lambda}$  in the principal component directions for the melt inclusion compositions. The small ellipse drawn with a solid line represents the projection of the whole rock principal components for La, Ce, Nd, Sm, Eu, Dy, Er, and Yb onto the melt inclusion principal components. The whole rock principal components are rotated  $\sim 25^\circ$  anticlockwise from the melt inclusion principal components. (e) Projection of melt inclusion compositions onto the melt inclusion REE eigenvectors given in Table 4. The fractional melt compositions are shown in the same way as in Figure 4b.

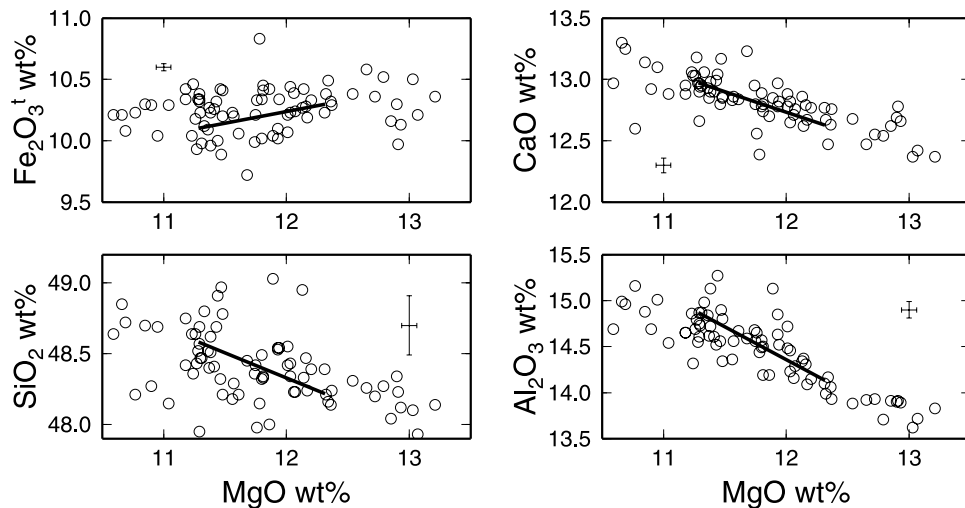


**Figure 5.** Element-element plots for Borgarhraun whole rock compositions. Circles show the sample compositions. The thick solid lines show the first principal component of length  $2\sqrt{\lambda_1}$  for the depleted mantle normalization (Table 5) projected onto the planes shown by the labels on the axes, corresponding to addition/removal of 8% the material shown in Table 6. The error bars show  $3\sigma$  precision estimates.

mantle source reduces the importance of MgO variability when it is used as a normalization composition. The second principal component for the sample average normalization is dominated by Fe variation, while the second principal component for the source normalized samples is nearly parallel to Ca.

[26] The composition and modal mineralogy of the material that was removed/added to produce the variability in major elements in the Borgarhraun samples can be estimated once the eigenvectors are known. The minimization routine described by *MacLennan et al.* [2001] was used to find the modal mineralogy of the material which best fit the principal components. When crystals separate from given batch of magma the average composition of the magma is altered and therefore the projection of the magma composition onto the principal components is also changed. The effect of removal of a single mineral type from the average sample composition can be shown as a vector whose length is controlled by the amount of the mineral removed from the original magma. Such vectors are shown in Figure 6 and are marked with the mineral name. If the mineral is added to the magma rather than removed, then the vector will point in the opposite direction. The vectors which represent addition/removal of minerals can be added in varying proportions to produce a vector ( $\mathbf{t}$ ) that is parallel to one of the principal components,  $\mathbf{u}_n$ , and has a length of  $\sqrt{\lambda_n}$ .

[27] The average Borgarhraun mineral compositions used in the fitting and the results of the fitting are shown in Figure 6 and Table 6. The mineral compositions are taken from *MacLennan et al.* [2001] and were normalized in the same way as the sample compositions. For both normalizations the first principal component corresponds to an olivine-rich material, with 60–85% olivine, 15–30% clinopyroxene and 0–12% plagioclase. This material has a similar modal mineralogy to that estimated for the phenocryst content of the samples by point counting (section 2). An olivine-gabbro can fit the second principal component for the sample average normalization. The weight fraction of

removal/addition of the material required to change the composition by one standard deviation ( $\sqrt{\lambda}$ ) is under 5% for both principal components. The total range in the first principal component can be matched by 24% addition/removal of the olivine-rich material.

[28] Over 90% of the variation in the concentration of major elements in the whole rock samples can be accounted for by addition/removal of crystals which are found in the lava. The relative importance of crystal removal (by fractional crystallization) and crystal addition (by incorporation of the material in magma chamber walls) is not yet clear but can be estimated using some of the methods outlined below.

[29] The variation in the first principal component of the samples shown in Figure 6 can be produced by variable amounts of accumulation of an olivine-rich material in a liquid with  $\sim 10.7$  wt % MgO. However, inspection of the hand specimens and the major element compositions shows that crystal accumulation alone does not produce the first principal component trend for the major elements. The hand specimen of sample FH9858 has  $\sim 20\%$  olivine crystals (point counting of the thin section showed 18.2%) and an MgO content of 11.86 wt %, while sample FH9826 is almost devoid of crystals in hand specimen (2% olivine by point counting) and has an MgO content of 12.03 wt %. If crystal abundance alone controlled the sample composition, then an increase in olivine content should raise the MgO content. The two samples described above show the opposite behavior. Both of these samples are fairly homogeneous and the portions of the sample that were crushed for analysis were representative of the sample as a whole. Therefore the first principal component trend is likely to be the result of both addition and removal of crystals from the magma.

[30] The Mg # of olivine and clinopyroxene in equilibrium with liquid that has the composition of the Borgarhraun whole rock samples was calculated using the methods of *Ford et al.* [1983] and *Putirka* [1999], and the results are shown in Figure 7. About 65% of the observed olivine compositions and 75% of the clinopyroxene compositions

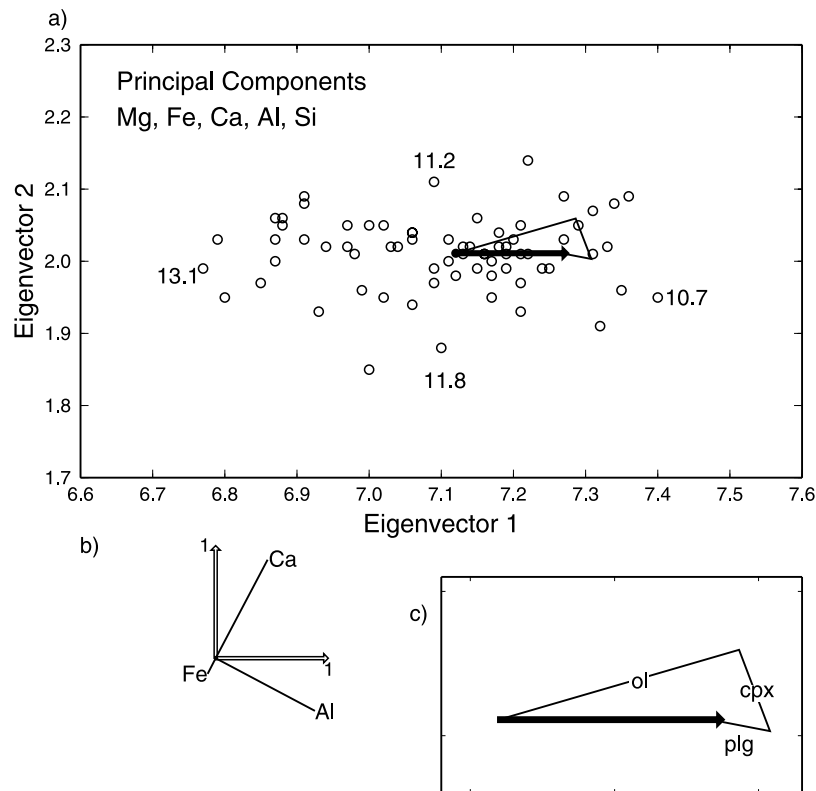


**Figure 6.** (a) Best fit to first principal component for major element compositions. The circles show the projection of the Borgarhraun whole rock sample compositions onto the principal components for the depleted mantle source normalization shown in Table 5. The MgO content of selected samples in wt % is shown. The thick solid arrow shows the best fit vector  $\mathbf{t}$  to the first principal component, which has a length of  $\sqrt{\lambda_1}$ . The origin of this arrow is at the average sample composition. The thin solid lines show the effect of removing minerals with the compositions and proportions given in Table 6. (b) Projection of selected elemental axes onto the first two principal components from Figure 6a. Arrows show unit vectors parallel to the principal components. (c) Magnification of best fit vector  $\mathbf{t}$  and vectors which correspond to removal of individual minerals. The minerals are removed in the order olivine, clinopyroxene, and plagioclase for clarity. The vector sum is not dependent on the order of removal.

are in Mg-Fe equilibrium with melts that have the composition of the Borgarhraun whole rock samples. However, ~20% of the olivine and clinopyroxene crystals have Mg # that are too high to have been in equilibrium with the whole rock compositions and were in equilibrium with more primitive compositions. Since the crystal compositions have a bimodal distribution, with separate peaks at Mg # of 88 and 91, it is possible that the high Mg # crystals were incorporated into the Borgarhraun melt from the walls of a magma body, while the lower Mg # crystals are the products of fractional crystallization from melts that had a similar or more evolved composition than that of the Borgarhraun whole rock samples. The presence of gabbroic and wehrlitic nodules in parts of the flow also suggests that material was incorporated into the magma from the walls of a magma body. Once again, these observations show that both crystal accumulation and fractional crystallization are likely to have influenced the major element composition of the Borgarhraun samples.

### 6. Mixing Process

[31] The range of REE compositional variability present in the olivine-hosted melt inclusions reflects compositional

**Table 6.** Fits to Principal Components<sup>a</sup>

	SiO <sub>2</sub>	Al <sub>2</sub> O <sub>3</sub>	FeO	MgO	CaO	Ol	Cpx	Plg	F
	<i>Compositions A</i>								
Ol	40.34	0.05	9.46	49.50	0.30	-	-	-	-
Cpx	51.52	4.86	3.88	17.96	20.26	-	-	-	-
Plg	46.36	33.77	0.35	0.23	17.82	-	-	-	-
	<i>Fit B</i>								
$\mathbf{u}_1$	44.53	5.33	6.69	34.07	8.54	57.4	31.5	11.2	4.0
$\mathbf{u}_2$	48.20	12.36	3.79	18.08	16.27	16.5	54.8	28.7	3.1
	<i>Fit C</i>								
$\mathbf{u}_1$	42.14	0.82	8.57	44.43	3.51	83.9	16.1	0.0	1.9
$\mathbf{u}_2$	47.17	18.01	3.10	14.65	15.76	16.6	35.1	48.3	3.0

<sup>a</sup>The mineral compositions in A used for fitting principal components are the average values for Borgarhraun minerals from MacLennan *et al.* [2001]. Fits B and C are the composition and modal mineralogy of fits to principal components for depleted mantle source normalized and sample average normalized, respectively. Fits to the eigenvectors shown in Table 5 using mineral compositions in A. The entries for Ol, Cpx, and Plg show the percentage of olivine, clinopyroxene, and plagioclase in the best fitting material.  $F$  is the weight percentage of material that must be added or removed in order to match the size of the eigenvalue. Weighting factors of  $w_1 = 0.1$ ,  $w_2 = 100$  and  $w_3 = 20$  were used for all runs [MacLennan *et al.*, 2001].

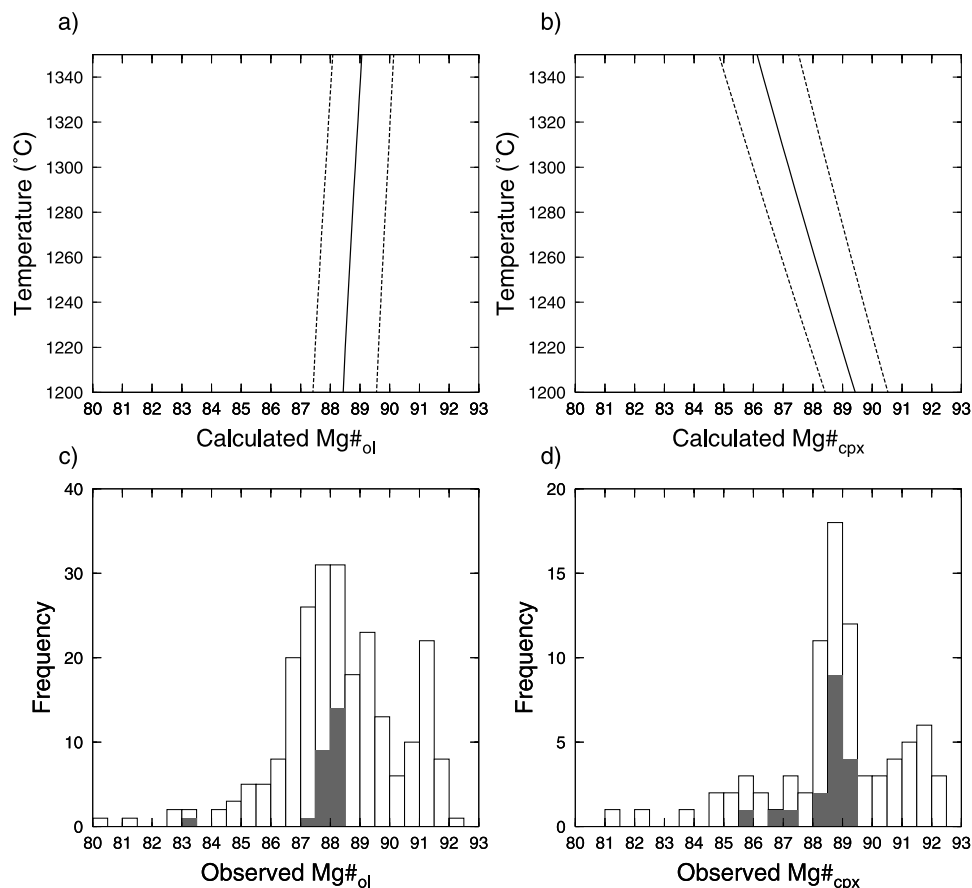


**Figure 7.** Borgarhraun olivine and clinopyroxene compositions. (a) Calculated Mg # for olivines in equilibrium with Borgarhraun whole rock compositions. Equilibrium olivine was calculated using the expressions from *Ford et al.* [1983], which gives the  $K_d^{Fe-Mg}$  as a function of liquid composition, pressure and temperature. The equilibrium olivine composition is shown for the average Borgarhraun composition with a solid line and for the extreme whole rock compositions with dashed lines. The calculations were carried out at 1 GPa, but the effect of pressure is negligible. (b) Calculated clinopyroxene compositions in equilibrium with Borgarhraun samples using the method of *Putirka* [1999]. The results shown are for 1 GPa; using atmospheric pressure reduces the calculated Mg # by  $\sim 1$ . (c) Histogram of observed olivine compositions from Borgarhraun samples. The dark shading shows the composition of the olivine in a nodule from sample FH9876. (d) Histogram of observed clinopyroxene compositions in Borgarhraun.

variability in the melts that the olivine crystals grew from. This variability is far greater than that found in the whole rock samples and it is clear from Figure 4 that mixing of batches of melt with the compositions of the melt inclusions can reproduce the variability found in the whole rock samples. Another important observation is that the mean of the melt inclusion compositions is similar to that of the whole rock samples, as would be expected if the whole rock samples are mixtures of melts with the compositional range of the melt inclusions (Figure 2).

### 6.1. Depth of Mixing

[32] It is possible to estimate the depth and temperatures at which melt mixing took place using the composition of olivine and clinopyroxene crystals in the samples along with the composition of the whole rock samples themselves. The pressures and temperatures of crystallization of olivines and clinopyroxenes present in the Borgarhraun samples was estimated by *MacLennan et al.* [2001], who used the olivine-

melt thermometer of *Roeder and Emslie* [1970], the clinopyroxene-melt thermometer and barometer of *Putirka et al.* [1996] and the clinopyroxene only barometer of *Nimis and Ulmer* [1998]. The thermobarometry and the associated uncertainties are discussed in detail by *MacLennan et al.* [2001].

[33] The olivine-melt and clinopyroxene-melt equilibrium temperatures calculated for Borgarhraun samples by *MacLennan et al.* [2001] lie in the range 1257–1343°C. Some of the Borgarhraun clinopyroxenes have Al<sub>2</sub>O<sub>3</sub> contents of over 5.5 wt %, indicative of high pressure origin. The equilibrium pressures calculated using the *Putirka et al.* [1996] clinopyroxene-liquid barometer lie in the range 0.8–0.9 GPa, and *MacLennan et al.* [2001] showed that errors caused by the use of the whole rock composition as an estimate for the liquid composition and the presence of clinopyroxene zonation are  $< 0.17$  GPa. Additional evidence that the clinopyroxenes last equilibrated at high pressures comes from the barometer of *Nimis and Ulmer* [1998]

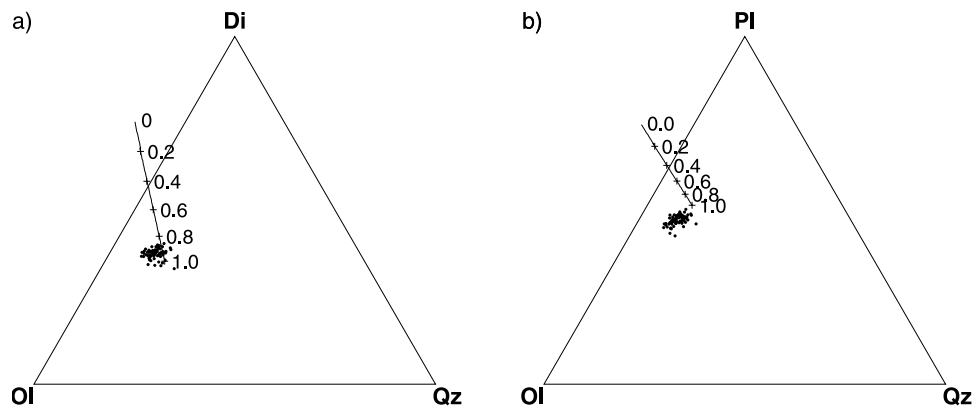


**Figure 8.** Borgarhraun whole rock samples and olivine-plagioclase-augite-melt (OPAM) boundary. Projections are from (a) plagioclase and (b) diopside and are calculated using the scheme of Walker *et al.* [1979]. The dots show the compositions of the Borgarhraun whole rock samples. The solid line shows the position of the OPAM saturation boundary predicted using the method of Yang *et al.* [1996], which is sensitive to pressure and the  $\text{SiO}_2$ ,  $\text{TiO}_2$ ,  $\text{K}_2\text{O}$ , and  $\text{Na}_2\text{O}$  contents of the melt. The average Borgarhraun composition was used for the melt, and the tick marks and values on the line show the effect of pressure (in GPa) on the position of the OPAM boundary.

which relies on the composition of the clinopyroxenes alone and returns pressures of 0.3–0.6 GPa. Furthermore, the experimental calibration of Nimis and Ulmer [1998] underestimates the equilibration pressure by 0.5 GPa for melts with compositions similar to those of the Borgarhraun samples.

[34] The methods of Yang *et al.* [1996] were used to estimate the pressure at which liquid with the composition of the whole rock samples are in equilibrium with olivine, plagioclase and clinopyroxene (referred to as the OPAM boundary). Figure 8 shows that the whole rock compositions lie close to predicted position of the OPAM boundary at pressures of 0.8–1.0 GPa. The scatter in the projected whole rock compositions can be produced by olivine accumulation in the samples.

[35] The simplest interpretation of these pressure estimates is that melt mixing took place at depths of 20–30 km, close to or deeper than the base of the crust (~20 km) under Theistareykir. Melts of variable REE composition may have ponded at this depth and then been trapped in growing olivine and clinopyroxene crystals. Melt inclusions hosted in Borgarhraun clinopyroxenes have a similar compositional range to olivine hosted melt inclusions [Slater *et al.*, 2001]. After inclusion entrapment, extensive melt mixing may have taken place at the same depth before rapid supply of melt to the Earth's surface for eruption. Alternatively, the melt inclusions may have been trapped in their host crystals at even greater depth, before they were carried to 20–30 km where the olivine and clinopyroxene equilibrated with the Borgarhraun melt. Furthermore, if extensive mixing of melt can occur without cooling and crystallization, then the OPAM pressure estimates only give a maximum estimate of the depth of mixing.

## 6.2. Extent of Mixing

[36] The variability of the melt inclusion and whole rock compositions can be used to estimate the extent of mixing. If the whole rock compositions represent mixed random samples of  $N$  melt inclusions from the population of melt

inclusions, then the value of  $N$  is given by the standard relationship  $N = (\sigma_M/\sigma_W)^2$ , where  $\sigma_M$  is the true standard deviation of the melt inclusion compositions and  $\sigma_W$  is the true standard deviation of the whole rock compositions [Slater *et al.*, 2001; Hoel, 1962]. The Ce content gives a value of  $N$  of ~27, while the first principal component for the REEs gives  $N \approx 21$  (the principal components used were those of the melt inclusions).

[37] However, Figure 4d shows that the ellipse which represents the variation in the whole rock compositions is smaller than that which represents the melt inclusion variability, and the whole rock first principal component axis is rotated anticlockwise by  $25^\circ$  from those of the melt inclusions. If the mixing process involved random sampling of the melt inclusion compositions (which was one of the assumptions involved in the calculation of  $N$ ), then the principal components of the whole rock samples and the melt inclusions should be parallel. Slater *et al.* [2001] showed that it was possible to model the mixing of fractional melts to produce the melt inclusion and whole rock compositions by varying the residual porosity in the melting column. The residual porosity contains the melt that remains in equilibrium with the mantle residue during near-fractional melting. The size and orientation of the principal axes of the observed Borgarhraun variability can be matched with a model residual porosity of 7% for the melt inclusions and 20% for the whole rock. However, increasing the residual mantle porosity during near-fractional melting is not likely to be the mixing process for Borgarhraun melts; U series disequilibrium observed in basalts from mid-ocean ridges requires residual porosities of ~0.1% [Richardson and McKenzie, 1994].

[38] The angle between the REE principal components of the melt inclusion and whole rock compositions may also reflect temporal changes in the average composition of the magma supplied to a chamber. Figure 9 shows that the melt inclusions trapped in olivines with a Mg # over 90.5 have a more restricted range in La/Yb than those found in lower Mg # olivines. The Kolmogorov-Smirnov test [Press *et al.*,

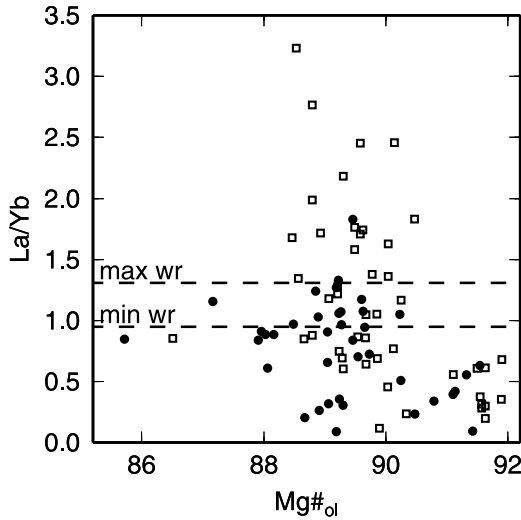


**Figure 9.** Borgarhraun melt inclusion compositions as a function of host olivine Mg #. Solid circles show measurements made in February 1999, while open squares show data from Slater *et al.* [2001]. The dashed lines show the compositional range found in Borgarhraun whole rock samples.

1992] was used to determine whether the sets of melt inclusions trapped in the high and low Mg # olivines come from the same population. The probability that the two sets come from the same population returned by the test was  $<2 \times 10^{-8}$  for La/Yb values. The highest La/Yb ratio of the melt inclusions trapped in the high Mg # olivines is 0.62, while the less forsteritic olivines contain melt inclusions with La/Yb  $> 3$ .

[39] The high Mg # olivines crystallized in an environment where melts with a high La/Yb ratio were not available for entrapment. High La/Yb melts are generated during the earliest stages of fractional melting in the garnet-stability field, while fractional melts with the lowest La/Yb ratios are produced at high degrees of melting at shallow depths ( $<80$  km) where garnet is not stable. If the average composition of the melt available for mixing changes with time, then the variability in the whole rock compositions cannot be described simply by random mixing of all the melt inclusion compositions. There is then no reason why the principal components of the melt inclusions and whole rock compositions should be colinear. However, the high Mg # olivines may not have crystallized from the parental magma to Borgarhraun so the change in average melt composition trapped in the olivines may not reflect changes in the magma chamber that supplied Borgarhraun. The change may instead be due to different average melt compositions in magma chambers that existed at similar depths but at different times.

## 7. Spatial Variability

[40] The geochemistry of samples from Borgarhraun is variable on all scales that can be resolved in this study, from over 10 km separation of samples to  $<5$  m. This behavior is evident from inspection of maps of the variability (e.g., Figure 10) and from smaller-scale examples. Even samples

FH9825 (Zr = 28.9 ppm) and FH9826 (Zr = 3 2.1 ppm), separated by  $<2$  m in a fissure, have significantly different compositions (Zr is 2.9 ppm different, while the standard deviation of measurement for Zr is  $\sim 0.3$  ppm). This difference is not the result of crystal accumulation in the magma. Zr is incompatible in all of the Borgarhraun phenocryst phases, including chrome-spinel [Horn *et al.*, 1994], so crystal accumulation will only act to dilute the Zr content in a sample. Olivine is the only phenocryst phase present in sufficient quantities in Borgarhraun samples to have a significant effect upon Zr concentration, but both point-counting results and the MgO contents of FH9825 (13.07 wt % MgO) and FH9826 (12.03 wt % MgO) show that olivine accumulation is not likely to be the cause of the variation in Zr content. The shift in MgO content can be produced by  $<3\%$  olivine accumulation, while the Zr contents vary by  $\sim 11\%$ . Hence Borgarhraun is not geochemically homogeneous or made up of large homogeneous packets of magma. Areas of the flow where the variability of the incompatible element concentrations appears to be small can be identified in Figure 10. For instance, there is little variation in the Zr concentration in the area around the crater, in the limbs at the extreme north and south of the flow and in the central western part of Borgarhraun. It is important to quantify the spatial heterogeneity in geochemistry and to assess whether these variations are significant. As described below, the root-mean-square (RMS) difference between sample compositions was used for this purpose. The composition of the samples varies with position, so the concentration of element  $k$  in the  $i$ th sample can be defined as  $c_i^k(\mathbf{r}_i)$  where  $\mathbf{r}_i$  is the vector which describes the sample location. For 70 samples, there exist 2415 sample pairings and the sample separation  $r_{ij}$  was calculated for each pairing:

$$r_{ij} = |\mathbf{r}_i - \mathbf{r}_j|. \quad (1)$$

The sample pairings were then binned using the value of  $r_{ij}$  by defining  $B_m(r_{ij})$

$$B_m(r_{ij}) = \begin{cases} 1 & (m-1)\Delta R < r_{ij} < m\Delta R, i \neq j, \\ 0 & \text{otherwise.} \end{cases} \quad (2)$$

where  $m$  is an integer with  $m = 1, 2, \dots, M$ . The results shown below use  $\Delta R = 2$  km so that sample pairings with a separation between 0 and 2 km fell in one bin, pairs with a separation between 2 and 4 km were grouped in the next bin, and so on up to the maximum separation of 12 km. This bin range was chosen since it best displays the length scale of the geochemical variation. With smaller bin ranges, the length scale of the variability was still clear, but the number of sample pairings in each bin dropped. The use of larger bin sizes could not resolve the length scale of the variability. The RMS difference in composition between paired samples in a distance bin centered on  $(m-1/2)R$  is  $\alpha_m$ , where

$$\alpha_m = \left[ \frac{\left( \sum_{i=1}^N \sum_{j=i}^N B_m(r_{ij})(c_i - c_j)^2 \right)}{\left( \sum_{i=1}^N \sum_{j=i}^N B_m(r_{ij}) \right)} \right]^{1/2} \quad (3)$$

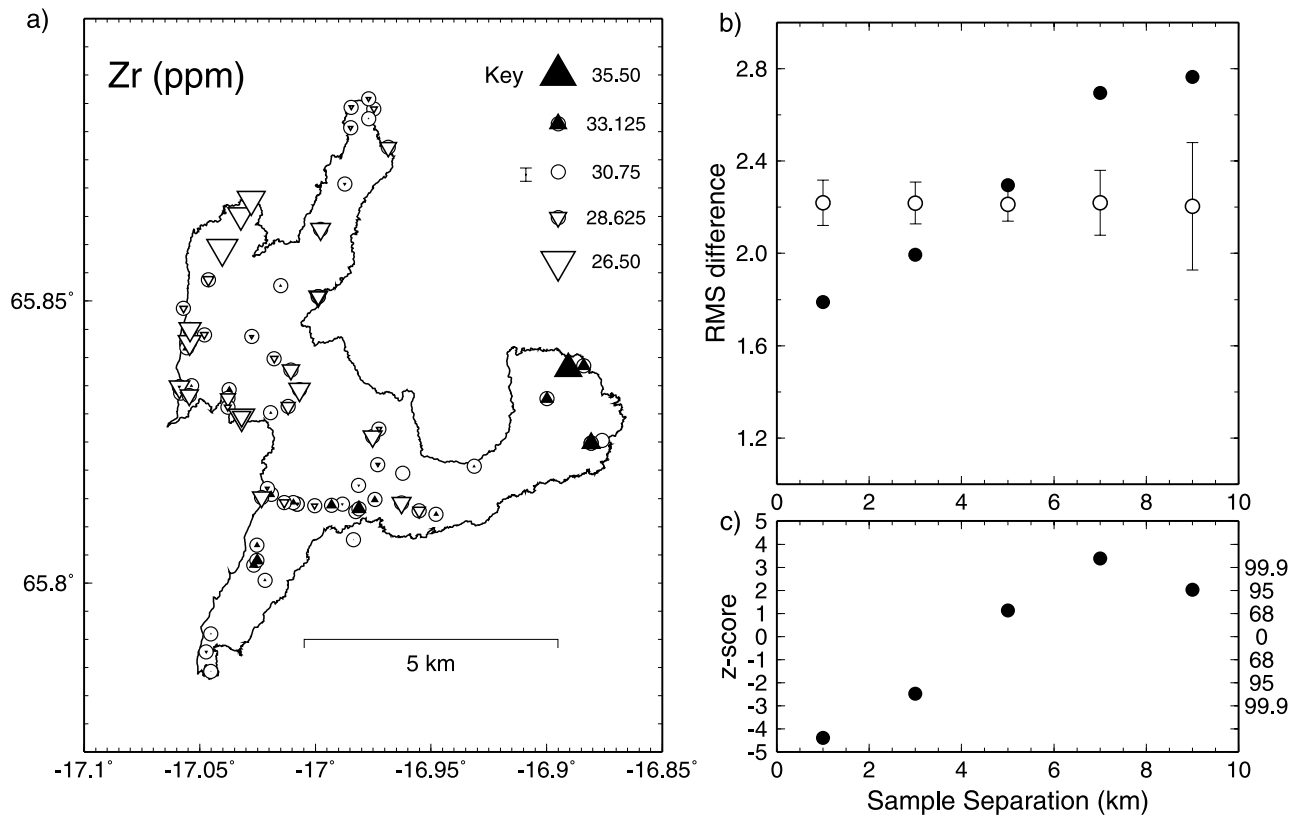


**Figure 10.** Spatial variation of whole rock Zr concentration. (a) Borgarhraun flow outline. Each sample location is shown as a triangle on a circle. Solid triangles show samples that have Zr concentrations that are greater than the average, and inverted open triangles show samples that have concentrations lower than the average (as shown on the scale). The larger the triangle, the more extreme the composition, so that the sample with the highest concentration is shown by the large solid triangle, but the average composition is shown as an open circle. (b) The RMS difference,  $\alpha_{Zr}$  from equation (3), plotted as a function of sample separation. Solid circles show the observed distribution, while open circles show the average for 1000 random distributions,  $\mu_z$ . The error bars show the standard deviation,  $\sigma_z$ , for the 1000 random distributions of geochemistry. See text for details. The increase at large separations occurs because there are fewer sample pairings at these distances. (c) The z score for the observed distribution as a function of sample separation shown by solid circles. This z score was calculated using the values shown in Figure 10b, and the expression  $z = [\alpha_{Zr} - \mu_z]/\sigma_z$ . The probability that the distribution is nonrandom at a given sample separation is marked on the right-hand axis. See text for further details.

and  $N$  is the total number of samples,  $c_i$  is the composition of the first sample in the pair and  $c_j$  is the composition of the second sample. The  $\alpha_m$  can be used to quantify the spatial variability observed within the Borgarhraun samples, as shown in Figures 10 and 11. This quantity is the square root of the variogram estimator, which is widely used in the analysis of spatial data [Matheron, 1962; Cressie, 1993]. For elements such as Zr it is clear that  $\alpha_m$  is smaller at short sample separations than it is at longer separations.

[41] It is important to determine if variation in  $\alpha_m$  is caused by a nonrandom distribution of sample compositions in Borgarhraun. It is possible to test whether the observed  $\alpha_m$  is likely to be random if the mean and standard deviation of  $\alpha_m$  for random spatial distributions of sample concentration are known and these values were estimated by producing 1000 synthetic random distributions of sample chemistry in the flow. Since the observed data consists of seventy sample collection points and seventy sets of geochemical measurements each sample location  $\mathbf{r}_i$  can be

numbered with  $i$  from 1 to 70 and each sample geochemistry  $c_j$  can be numbered with  $j$  from 1 to 70. The sample compositions were randomly reallocated to the sample locations using the random number generator RAN1 from Press *et al.* [1992]. RAN1 was used to obtain a random integer  $l$  with a value between 1 and 70, and the first composition ( $j = 1$ ) was assigned to the  $l$ th sample location ( $\mathbf{r}_l$ ). This sample was removed from the list of locations, leaving 69 available locations. Then RAN1 was used to give  $l$  with a value between 1 and 69 and the second sample composition ( $j = 2$ ) was assigned to the  $l$ th remaining sample location. This reallocation continued until all the sample compositions had been assigned locations.

[42] Once a random reallocation of all the samples had been made,  $\alpha_m$  was calculated for the resulting distribution. The mean,  $\mu_z$ , and standard deviation,  $\sigma_z$ , of  $\alpha_m$  for random spatial distributions of composition were obtained from 1000 repeats of the random reallocation of samples. These estimates are shown along with the observed  $\alpha_m$  in Figures 10

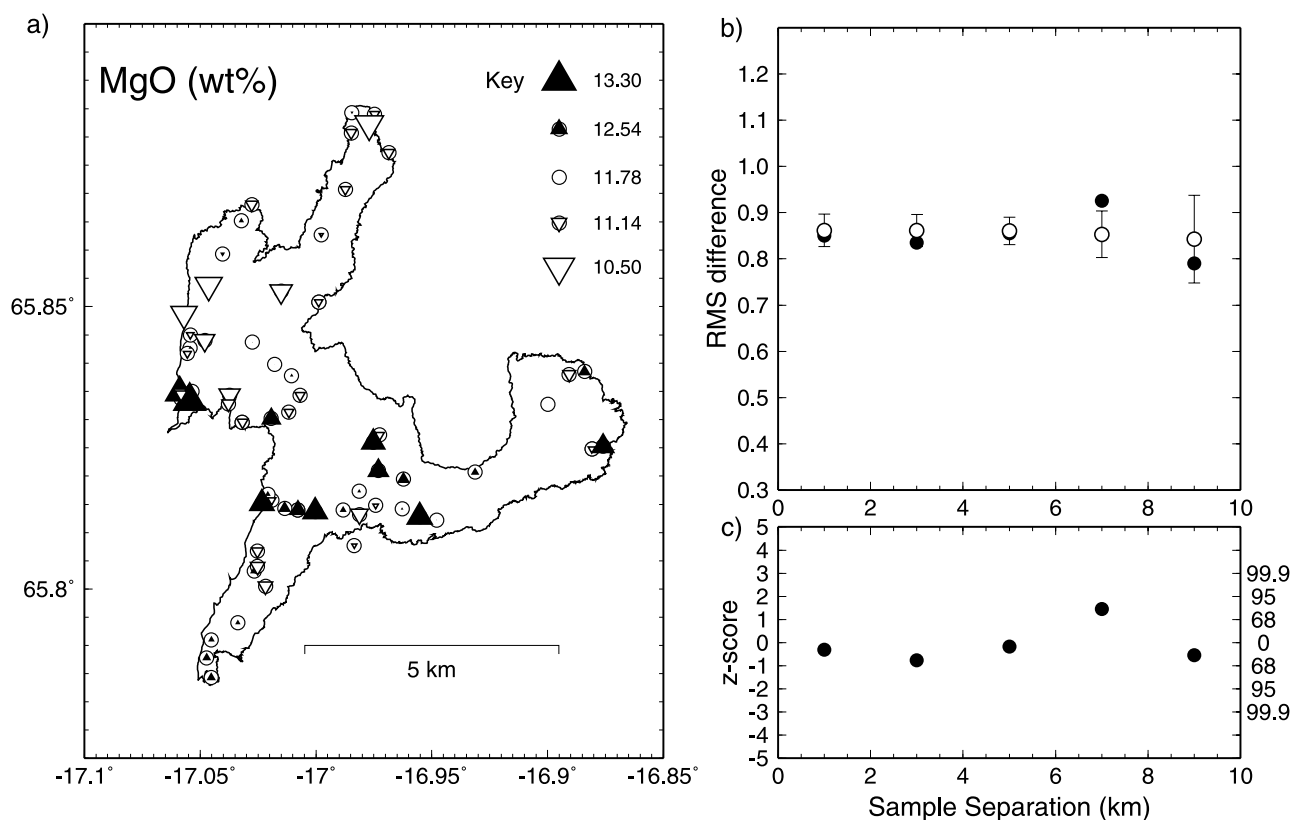


**Figure 11.** Spatial variation of MgO content (wt %) with same key as Figure 10.

and 11. A measure of the likelihood that the observed  $\alpha_m$  is random is the  $z$  score, which is calculated for each bin using  $z = [\alpha_m - \mu_z]/\sigma_z$ . If the RMS difference in sample compositions for a given bin is less than that for a random distribution, then  $z$  will be negative, and if the RMS difference in sample compositions for a given bin is greater than that for a random distribution, then  $z$  will be positive. If the value of  $z > 2$  or  $z < -2$  for a given bin, then there is a 95% probability that the geochemistry is not randomly distributed at the length scale of the bin. The relationship between  $z$  and probability is tabulated in many standard statistical textbooks [e.g., *Kreyszig*, 1993, Table A8, p. A102].

[43] For Zr, Nd and the first principal component of the REEs,  $\alpha_m$  is significantly lower than that expected for random distributions at separation distances of  $<4$  km. Figure 10 shows the distribution for Zr, which is typical of that of a number of incompatible elements. The  $z$  scores for Zr are as low as  $-4.4$  at small sample separations, corresponding to a chance of one in a million of the observed distribution being random. At sample separation greater than 4 km the  $z$  scores become positive as the observed  $\alpha_m$  increases. A similar pattern is also observed for the Zr/Y ratio with  $z$  scores of  $-3$  at separations  $<4$  km. However, the spatial pattern for MgO concentration and other compatible elements is quite different to that for incompatible elements (Figure 11). The  $z$  scores for MgO concentration lie in the range from  $-1$  to  $1.5$  for all of the bins. When the magnitude of the  $z$  score is 1.5, there is a 14% chance that the observed distribution is random. For the 0–2 km bin the  $z$  score for MgO is close to  $-0.3$ , which corresponds to a 76% probability that the distribution is

random. Therefore, it is not clear that the compatible elements have any nonrandom spatial structure to their geochemical variability over the length scales considered. If such structure does exist for the compatible elements, then it is much weaker than that observed for incompatible elements.

[44] The  $z$  score results at 0–4 km sample separation are summarized in Figure 12. The effective partition coefficient in the melting region,  $D_m$ , was calculated by dividing the concentration of the element in the depleted source by the predicted melt composition from the Theistareykir melting model of *Slater et al.* [2001]. The most incompatible elements show  $z$  scores close to zero for the separation distances and bin sizes considered here and their spatial variability is not significantly different to that of a random distribution. Most of the moderately incompatible elements ( $0.15 < D_m < 0.25$ ) have  $z$  scores lower than  $-2$  at sample separations under 4 km, while more compatible elements have random spatial variability.

[45] It has been shown in a previous section that the variability in the incompatible elements can be accounted for by incomplete mixing of fractional melts, while the major element variability can be explained by addition/removal of the crystals found in the lava. The fractional crystallization and wall rock assimilation which control the major element concentrations have not left a strong spatial signature on the lava on the scale of kilometers, although there may be short wavelength structure which cannot be resolved by the sampling density of this study. In contrast, many of the elements whose concentrations are primarily controlled by the mixing of fractional melts

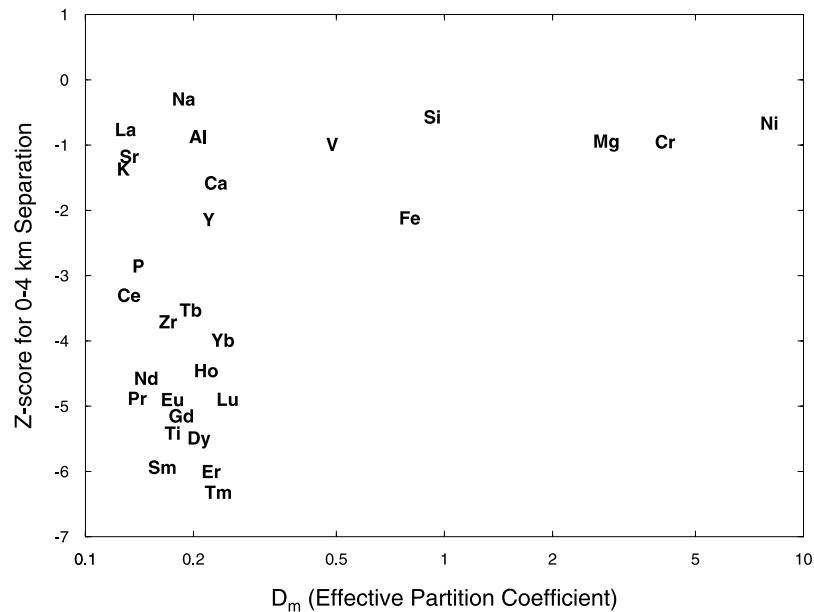


**Figure 12.** The  $z$  scores for spatial variability at sample separations between 0 and 4 km plotted against the effective melt/mantle partition coefficient ( $D_m$ ) which is calculated as described in the text and plotted on a log scale. The element name is written at the appropriate position and elements with a signal-to-noise ratio of  $<1$  are not plotted.

have structure in their spatial variability, so that samples separated by  $<4$  km are more similar than expected from a random distribution. If circles with a diameter of 4 km are placed with their centers on the sample positions, then on average about one half of the area of the circle is filled with flow, so that the average area of flow contained within each circle is  $\sim 7$  km<sup>2</sup>.

[46] In order to estimate the volume of magma associated with a sample separation of 4 km, both the flow thickness and the vertical distance over which the compositional differences become greater than random need to be known. The base of Borgarhraun is not clearly exposed in the fissures which run through the central part of the flow, so the thickness cannot be directly measured. Some of the fissures are  $\sim 5$  m deep, so parts of Borgarhraun have at least this thickness. Dissected lava flows which are exposed in the active volcanic zones and the Tertiary sections of Iceland seldom have thicknesses of  $>20$  m, so it is not likely that Borgarhraun is thicker than this. Because the base of the flow is not exposed and detailed vertical sampling was not undertaken, a direct measure of the vertical changes in composition within the flow is not yet available. Although most of the samples were taken from the surface of the flow, 30 were taken from fissure walls between 0.5 and 5.0 m beneath the flow surface and these samples allow a crude estimate of the relationship between depth beneath the flow surface and composition to be made. The  $z$  score for variability in Zr content in the 0–2 km bin is  $-4.38$  with all sample pairs. If only sample pairs where one sample is from the flow surface and one sample is from a fissure are included in the analysis, then the  $z$  score is  $-3.77$  and the switch from negative to positive  $z$  scores takes place at a separation distance of  $\sim 4$  km. This behavior implies that the variations in composition with depth in the surface part of the flow including the flow surface and the uppermost few

meters where most of the fissure samples were taken are not strong enough to obscure the nonrandom horizontal variations in geochemistry that are present in the flow. Therefore the vertical coherence length is likely to exceed 2 m. Thus parts of the flow that show correlated variations in the incompatible element concentrations have an area of  $\sim 7$  km<sup>2</sup> and a volume of between 0.014 and 0.14 km<sup>3</sup>.

## 8. Discussion

[47] The variability of the REE contents of melt inclusions and whole rock samples can be produced by incomplete mixing of fractional melts, whereas that of the major elements is likely to result from fractional crystallization and wall rock assimilation in sub-Moho magma bodies. It is possible that the melt bodies in which mixing took place are similar to those that are thought to have produced the Moho transition zone (MTZ) gabbros in Oman [Korenaga and Kelemen, 1997]. The spatial structure observed in the geochemical variation presumably reflects aspects of the mixing process in both the magma bodies and in the melt conduits which supplied them. The moderately incompatible elements show a spatial structure where samples separated by  $<4$  km have more similar compositions than expected from a random distribution of geochemistry in the flow. This sample separation corresponds to a magma volume of  $\sim 0.01$ – $0.1$  km<sup>3</sup>. In contrast, compatible elements show a random distribution of concentrations on length scales of kilometers. Therefore the 4 km scale variability is not the result of fractional crystallization or crystal accumulation in the flow.

[48] It is possible to model the Borgarhraun observations by mixing of fractional melts in a sub-Moho magma chamber and in this section a sequence of events is outlined which is compatible with these observations. First, melts

which are variable in composition are supplied to the chamber and are mixed by fluid motions and diffusion. At this stage crystallization of olivine from the magma entraps melt inclusions. The diffusion rate of REEs in basaltic liquids is  $\sim 10^{-11} \text{ m}^2 \text{ s}^{-1}$  [Leshner, 1994; LaTourrette et al., 1996], so in 1 year, diffusion alone can mix compositions over distances of  $\sim 0.02 \text{ m}$ . It will take far longer to homogenize a  $0.1 \text{ km}^3$  volume of magma. If this magma volume fills a spherical chamber, it will have a radius of  $\sim 300 \text{ m}$  and will take over 900 kyr to homogenize by diffusion alone. Stirring of the magma will greatly increase the rate of homogenization of the melt composition in the chamber and will act along with diffusion to reduce the compositional variability from that observed in the melt inclusions toward that of the whole rock samples. While mixing homogenizes the incompatible element composition of the magma, fractional crystallization and wall rock assimilation can produce variability in the major element concentrations. Differential movement of crystals and melt can also generate short wavelength variability in major element compositions. Stoke's law can be used to estimate the settling velocity,  $u$ , of crystals in melt by  $u = 2R^2 \Delta\rho g / 9\eta$ , where  $R$  is the crystal radius,  $\Delta\rho$  is the density contrast between the crystal and melt,  $g$  is acceleration due to gravity and  $\eta$  is the dynamic viscosity. This expression gives a settling velocity of  $\sim 0.01 \text{ m s}^{-1}$  for a spherical olivine crystal with a radius of  $0.5 \text{ mm}$  in basaltic liquid with  $\eta = 1 \text{ Pa s}$  and  $\Delta\rho = 500 \text{ kg m}^{-3}$ . Therefore differential movement of crystals and melt is likely to take place in the magma chamber. Although the sequence of the events is not well constrained by the observations, it is possible that mixing, fractional crystallization and assimilation were contemporaneous. The small-scale variability caused by crystal movement cannot be resolved by the sample spacing used in this study. The pattern of spatial variability observed in the incompatible elements can be produced if the magma chamber episodically supplies melt to the surface in batches of  $\sim 0.01\text{--}0.1 \text{ km}^3$  volume and these batches flow over the surface during eruptive events. Episodic fracturing of magma chamber walls is consistent both with field observations of fissure eruptions in northern Iceland and with simple physical models of magma bodies in the lower oceanic crust [Kelemen and Aharanov, 1998]. In the case of the most recent rifting episode at Krafla, there were nine eruptions over a time span of 9 years, with the repose time between eruptions ranging from 3 months to 3 years [Saemundsson, 1991].

## 9. Conclusions

[49] Variability is present above the estimated level of analytical noise for almost all measured elements in Borgarhraun whole rock samples. The REE variation in whole rock samples and melt inclusions can be produced by incomplete mixing of fractional melts generated by a melting model which matches the average lava composition and crustal thickness of Theistareykir.

[50] The melt inclusion compositions are more variable than the whole rock compositions and a simple mixing model shows that the magnitude of variability of the whole rock samples can be matched if each hand specimen is a sample of magma that was formed by mixing of 20–30

**Table 7.** Variability in Borgarhraun Whole Rock Samples<sup>a</sup>

	$\bar{x}$	$\sigma_o$	$\sigma_{rs}$	$\sigma_{rp}$	$\sigma_h$	$\sigma_t$	$\sigma_t/\sigma_{rs}$
Nb	1.67	0.07	0.11	0.10	0.04	–	–
Zr	31.26	1.54	0.18	0.17	0.06	1.53	8.80
Y	16.58	0.59	0.13	0.12	0.07	0.57	5.00
Sr	92.12	2.35	0.30	0.18	0.24	2.33	12.99
Rb	0.86	0.05	0.14	0.12	0.06	–	–
Zn	67.64	1.41	0.77	0.46	0.61	1.18	2.55
Cu	98.61	7.08	0.73	0.42	0.60	7.04	16.79
Ni	254.87	26.29	2.85	1.38	2.50	26.13	18.99
Cr	774.97	122.39	7.40	1.95	7.14	122.17	62.52
V	245.05	6.41	3.01	2.60	1.50	5.66	2.17
Ba	11.56	1.17	2.27	2.02	1.04	–	–
Sc	39.83	0.68	0.76	0.62	0.44	–	–

<sup>a</sup>Results of analyses of 10 Borgarhraun samples using a high-precision XRF machine. The mean of each sample was calculated from 6 repeats and the mean and standard deviation of the 10 samples are given by  $\bar{x}$  and  $\sigma_o$ . Calculation of the precision estimates  $\sigma_{rs}$ ,  $\sigma_{rp}$ , and  $\sigma_h$  is described in the text. The true sample variability,  $\sigma_t$ , and the signal-to-noise ratio,  $\sigma_t/\sigma_{rs}$ , were calculated as for Table 1, with the small difference that the  $\sigma_{rs}$  term used includes variation caused by powder heterogeneity.

batches of melt with the compositional variability of the inclusions. It is likely that part of the mixing took place in a sub-Moho magma body.

[51] The variability in major elements can be modelled by addition/removal of the olivine, clinopyroxene and plagioclase crystals found in the magma. About 75% of the olivine and clinopyroxene crystals are in equilibrium with liquids that have the composition of the Borgarhraun whole rock samples, while  $\sim 15\%$  are more primitive. Thermobarometry shows that the olivine and clinopyroxene compositions were in equilibrium with the whole rock composition at  $\sim 1300^\circ\text{C}$  and  $0.9 \text{ GPa}$  ( $\sim 30 \text{ km}$  depth). The whole rock compositions lie on the olivine-plagioclase-clinopyroxene-liquid phase boundary at similar pressures. Hence the major element variation can be produced by fractional crystallization and assimilation of cumulates in sub-Moho magma chambers.

[52] Analysis of the distribution of geochemistry in Borgarhraun shows that the spatial distribution of the concentrations of moderately incompatible elements is not random, so that samples with a separation of  $<4 \text{ km}$  have more similar concentrations than expected from a random distribution of geochemistry. This separation distance corresponds to a lava volume of  $0.014\text{--}0.14 \text{ km}^3$ . This volume may be controlled by magma mixing and episodic eruption of melts from a sub-Moho chamber. The concentration variations of compatible elements with position cannot be distinguished from random variation. It is likely that crystal removal and addition control major element variability on length scales that are smaller than the resolution of this study.

## Appendix A: High-Precision XRF Analyses

[53] Ten of the Borgarhraun samples were analyzed using a new high-precision XRF machine at the University of Edinburgh in June 2002 in order to confirm the presence of natural trace element variability in the flow and to better quantify the degree of compositional heterogeneity within the powders of single samples. Samples 01, 12, 21, 22, 28, 33, 37, 54, 71, and 77 were reanalyzed using a Phillips PW

2404 XRF spectrometer with a Rh-anode end-window X-ray tube, and operating conditions were similar to those described by *Fitton et al.* [1998]. Two powder pellets were prepared for each of the 10 samples, and 3 analyses were made of each pellet, giving a total of 60 analyses for each element. Precision estimates were then made using the method described in section 3.1. The six repeats of each sample were used to calculate  $\sigma_{rs}$ , a precision estimate which includes the effects of heterogeneous contamination during the pellet preparation, of powder inhomogeneity and of machine measurement noise. The three repeats of each pellet were used to calculate  $\sigma_{rp}$  which is an estimate of the machine noise alone. Then variability between different pellets of the same sample,  $\sigma_h$ , was estimated using  $\sigma_h^2 = \sigma_{rs}^2 - \sigma_{rp}^2$ .

[54] The results in Table 7 reinforce the conclusions of the earlier XRF work detailed in the main text, which show that geochemical variability is present in Borgarhraun. The use of the high precision XRF machine more than doubles the signal-to-noise ratio of incompatible trace elements such as Zr, Y and Sr. The  $\sigma_t$  values given for elements analyzed by XRF in Table 1 are not corrected for the possible effects of incomplete mixing of the sample powder before sample preparation or heterogeneous contamination, which are estimated here by  $\sigma_h$ . The effect of correcting  $\sigma_t$  from Table 1 with the  $\sigma_h$  from Table 7 is small for both for incompatible trace elements like Zr, Y and Sr and compatible trace elements such as Ni and Cr.

[55] **Acknowledgments.** The authors would like to thank Francis Nimmo and Iris van der Zander for their help in the field and Godfrey Fitton, Graham Layne, Stephen Reed, and the staff of the NERC ICP-MS facility at Silwood Park for assistance with the analyses. Judith Bunbury gave useful comments on an early version of the manuscript. Don Baker, Don Myers, John Fournelle, and an anonymous party gave thorough reviews which helped to improve the clarity of this paper. Don Baker and Francis Albarède gave helpful editorial advice. The Royal Society, NERC and NSF (grant EAR990400) are thanked for their financial assistance. This is Earth Sciences contribution 6733.

## References

- Albarède, F., *Introduction to Geochemical Modeling*, Cambridge Univ. Press, New York, 1995.
- Albarède, F., and Y. Bottinga, Kinetic disequilibrium in trace element partitioning between phenocrysts and host lava, *Geochim. Cosmochim. Acta*, **36**, 141–156, 1972.
- Anderson, A. T., Evidence for picritic, volatile-rich magma beneath Mt. Shasta, California, *J. Petrol.*, **15**, 243–267, 1974.
- Caroff, M., R. C. Maury, J. Cotten, and J.-P. Clément, Segregation structures in vapor-differentiated basaltic flows, *Bull. Volcanol.*, **62**, 171–187, 2000.
- Cressie, N. A. C., *Statistics for Spatial Data*, John Wiley, New York, 1993.
- Elliott, T. R., C. J. Hawkesworth, and K. Gronvöld, Dynamic melting of the Iceland plume, *Nature*, **351**, 201–206, 1991.
- Fitton, J. G., A. D. Saunders, L. M. Larsen, B. S. Hardarson, and M. J. Norry, Volcanic rocks from the southeast Greenland margin at 63°N: Composition, petrogenesis and mantle sources, *Proc. Ocean Drill. Program Sci. Results*, **152**, 331–350, 1998.
- Ford, C. E., D. G. Russell, J. A. Craven, and M. R. Fisk, Olivine liquid equilibria—Temperature, pressure and composition dependence of the crystal liquid cation partition coefficients for Mg Fe<sup>2+</sup>, Ca and Mn, *J. Petrol.*, **24**, 256–265, 1983.
- Goff, F., Vesicle cylinders in vapor-differentiated flows, *J. Volcanol. Geotherm. Res.*, **71**, 167–185, 1996.
- Govindaraju, K., 1994 compilation of working values and sample description for 383 geostandards, *Geostand. Newsl.*, **18**, 1–158, 1994.
- Grove, T. L., R. J. Kinzler and W. B. Bryan, Fractionation of mid-ocean ridge basalt (MORB), in *Mantle Flow and Melt Generation at Mid-ocean Ridges*, *Geophys. Monogr. Ser.*, vol. 71, edited by J. Phipps Morgan, D. K. Blackman, and J. M. Sinton, pp. 281–311, AGU, Washington, D. C., 1992.
- Gurenko, A. A., and M. Chaussidon, Enriched and depleted primitive melts included in olivine from Icelandic tholeiites—Origin by continuous melting of a single mantle column, *Geochim. Cosmochim. Acta*, **135**, 21–34, 1995.
- Hoel, P. G., *Introduction to Mathematical Statistics*, John Wiley, New York, 1962.
- Horn, I., S. F. Foley, S. E. Jackson, and G. A. Jenner, Experimentally determined partitioning of high-field strength-elements and selected transition-elements between spinel and basaltic melt, *Chem. Geol.*, **117**, 193–218, 1994.
- Jochum, K. P., H. M. Seufert, and M. F. Thirlwall, High sensitivity Nb analysis by spark-source mass spectrometry (SSMS) and calibration of XRF Nb and Zr, *Chem. Geol.*, **81**, 1–16, 1990.
- Johnson, K. T. M., H. J. B. Dick, and N. Shimizu, Melting in the oceanic upper mantle: An ion microprobe study of diopsides in abyssal peridotites, *J. Geophys. Res.*, **97**, 9219–9241, 1992.
- Kamenetsky, V. S., S. M. Eggins, A. J. Crawford, D. H. Green, M. Gasparon, and T. J. Falloon, Calcic melt inclusions in primitive olivine at 43°N MAR: Evidence for melt-rock reaction/melting involving clinopyroxene-rich lithologies during MORB generation, *Earth Planet. Sci. Lett.*, **160**, 115–132, 1998.
- Kelemen, P. B., and E. Aharonov, Periodic formation of magma fractures and generation of layered gabbros in the lower crust beneath oceanic spreading ridges, in *Faulting and Magmatism at Mid-ocean Ridges*, *Geophys. Monogr. Ser.*, vol. 106, edited by R. W. Buck et al., pp. 267–289, AGU, Washington, D. C., 1998.
- Kirkpatrick, R. J., Nucleation and growth of plagioclase, Makaopuhi and Alae lava lakes Kilauea Volcano, Hawaii, *Geol. Soc. Am. Bull.*, **88**, 78–84, 1977.
- Korenaga, J., and P. B. Kelemen, Origin of gabbro sills in the Moho transition zone of the Oman ophiolite: Implications for magma transport in the oceanic lower crust, *J. Geophys. Res.*, **102**, 27,729–27,749, 1997.
- Kreyszig, E., *Advanced Engineering Mathematics*, 7th ed., John Wiley, New York, 1993.
- Langmuir, C. H., E. M. Klein, and T. Plank, Petrological systematics of mid-ocean ridge basalts: Constraints on melt generation beneath ocean ridges, in *Mantle Flow and Melt Generation at Mid-ocean Ridges*, *Geophys. Monogr. Ser.*, vol. 71, edited by J. Phipps Morgan, D. K. Blackman, and J. M. Sinton, pp. 183–280, AGU, Washington, D. C., 1992.
- Lasaga, A. C., Implications of a concentration-dependent growth rate on the boundary layer crystal-melt model, *Earth Planet. Sci. Lett.*, **56**, 429–434, 1981.
- LaTourette, T., G. J. Wasserburg, and A. J. Fahey, Self diffusion of Mg, Ca, Ba, Nd, Yb, Ti, Zr and U in haplobasaltic melt, *Geochim. Cosmochim. Acta*, **60**, 1329–1340, 1996.
- Le Maitre, R. W., *Numerical Petrology: Statistical interpretation of geochemical data*, *Dev. Petrol.*, vol. 8, Elsevier Sci., New York, 1982.
- Leshner, C. E., Kinetics of Sr and Nd exchange in silicate liquids - theory, experiments, and applications to uphill diffusion, isotopic equilibration and irreversible mixing of magmas, *J. Geophys. Res.*, **99**, 9585–9604, 1994.
- Lindstrom, M. M., and L. A. Haskin, Compositional inhomogeneities in a single Icelandic tholeiite flow, *Geochim. Cosmochim. Acta*, **45**, 15–31, 1981.
- MacLennan, J., D. McKenzie, K. Gronvöld, and L. Slater, Crustal accretion under northern Iceland, *Earth Planet. Sci. Lett.*, **191**, 295–310, 2001.
- Matheron, G., *Traité de géostatistique appliquée*, Tome I, *Mém. BRGM*, **14**, 1962.
- McKenzie, D., and R. K. O’Nions, Partial melt distributions from inversion of rare earth element concentrations, *J. Petrol.*, **32**, 1021–1091, 1991.
- McKenzie, D., and R. K. O’Nions, Melt production beneath oceanic islands, *Phys. Earth Planet. Inter.*, **107**, 143–182, 1998.
- Nielsen, R. L., J. Crum, R. Bourgeois, K. Hascall, L. M. Forsythe, M. R. Fisk, and D. M. Christie, Melt inclusions in high-An plagioclase from the Gorda Ridge: An example of local diversity of MORB parent magmas, *Contrib. Mineral. Petrol.*, **122**, 34–50, 1995.
- Nimis, P., and P. Ulmer, Clinopyroxene geobarometry of magmatic rocks, part 1, An expanded structural geobarometer for anhydrous and hydrous, basic and ultrabasic systems, *Contrib. Mineral. Petrol.*, **133**, 122–135, 1998.
- O’Nions, R. K., R. J. Pankhurst, and K. Gronvöld, Nature and development of basalt magma sources beneath Iceland and the Reykjanes Ridge, *J. Petrol.*, **17**, 315–338, 1976.
- Perfit, M. R., and W. W. Chadwick Jr., Magmatism at mid-ocean ridges: Constraints from volcanological and geochemical investigations, in *Faulting and Magmatism at Mid-Ocean Ridges*, *Geophys. Monogr. Ser.*, vol. 106, edited by R. W. Buck et al., pp. 59–116, AGU, Washington, D. C., 1998.

- Press, W. H., B. P. Flannery, S. A. Teukolsky, and W. T. Vetterling, *Numerical Recipes*, 2nd ed., Cambridge Univ. Press, New York, 1992.
- Putirka, K., Clinopyroxene plus liquid equilibria to 100 kbar and 2450 K, *Contrib. Mineral. Petrol.*, *135*, 151–163, 1999.
- Putirka, K., M. Johnson, R. Kinzler, J. Longhi, and D. Walker, Thermobarometry of mafic igneous rocks based on clinopyroxene-liquid equilibria, 0–30 kbar, *Contrib. Mineral. Petrol.*, *123*, 92–108, 1996.
- Reed, S. J. B., *Electron Microprobe Analysis and Scanning Electron Microscopy in Geology*, Cambridge Univ. Press, New York, 1996.
- Reyment, R. A., and K. G. Jöreskog, *Applied Factor Analysis in the Natural Sciences*, Cambridge Univ. Press, New York, 1993.
- Rhodes, J. M., Homogeneity of lava flows: Chemical data for historic Mauna Loa eruptions, *J. Geophys. Res.*, *88*, A869–A879, 1983.
- Richardson, C., and D. McKenzie, Radioactive disequilibria from 2D models of melt generation by plumes and ridges, *Earth Planet. Sci. Lett.*, *128*, 425–437, 1994.
- Roeder, P. L., and R. F. Emslie, Olivine-liquid equilibrium, *Contrib. Mineral. Petrol.*, *29*, 275–289, 1970.
- Roedder, E., *Fluid Inclusions*, *Rev. Mineral.*, vol. 12, Mineral. Soc. of Am., Washington, D. C., 1984.
- Rogan, W., S. Blake, and I. Smith, In situ chemical fractionation in thin basaltic lava flows: Examples from the Auckland volcanic field, New Zealand, and a general physical model, *J. Volcanol. Geotherm. Res.*, *74*, 89–99, 1996.
- Rubin, K. H., M. C. Smith, E. C. Bergmanis, M. R. Perfit, J. M. Sinton, and R. Batiza, Geochemical heterogeneity within mid-ocean ridge lava flows: Insights into eruption, emplacement and global variations in magma generation, *Earth Planet. Sci. Lett.*, *188*, 349–367, 2001.
- Sæmundsson, K., *Jardfræði Kröflukerfisins*, in *Náttúra Mývatns*, edited by A. Gardarsson and A. Einarsson, pp. 24–95, Hid íslenska náttúrufræðifélag, Reykjavík, 1991.
- Shimizu, N., The geochemistry of olivine-hosted melt inclusions in a FAMOUS basalt ALV519-4-1, *Phys. Earth Planet. Inter.*, *107*, 183–201, 1998.
- Shimizu, N., and S. R. Hart, Applications of the ion microprobe to geochemistry and cosmochemistry, *Annu. Rev. Earth. Planet. Sci.*, *10*, 483–526, 1982.
- Sigmarrsson, O., M. Condomines, K. Grönvöld, and T. Thordarson, Extreme magma homogeneity in the 1783–84 Lakagigar eruption—Origin of a large volume of evolved basalt in Iceland, *Geophys. Res. Lett.*, *18*, 2229–2232, 1991.
- Slater, L., Melt generation beneath Iceland, Ph.D. thesis, Univ. of Cambridge, Cambridge, U.K., 1996.
- Slater, L., D. McKenzie, K. Grönvöld, and N. Shimizu, Melt generation and movement beneath Theistareykir N. E. Iceland, *J. Petrol.*, *42*, 321–354, 2001.
- Staples, R. K., R. S. White, B. Brandsdóttir, W. Menke, P. K. H. Maguire, and J. H. McBride, Färoe-Iceland Ridge Experiment, 1, Crustal structure of northeastern Iceland, *J. Geophys. Res.*, *102*, 7849–7866, 1997.
- Stracke, A., A. Zindler, V. J. M. Salters, D. McKenzie, J. Blichert-Toft, F. Albarède, and K. Grönvöld, Theistareykir revisited, *Geochem. Geophys. Geosyst.*, *3*, doi:10.1029/2001GC000201, in press, 2002.
- Walker, D., T. Shibata, and S. E. DeLong, Abyssal tholeiites from the Oceanographer Fracture Zone, *Contrib. Mineral. Petrol.*, *70*, 111–125, 1979.
- Watkins, N. D., B. M. Gunn, and R. Coy-yl, Major and trace element variations during the initial cooling of an Icelandic lava, *Am. J. Sci.*, *268*, 24–49, 1970.
- Watson, S., and D. McKenzie, Melt generation by plumes—A study of Hawaiian volcanism, *J. Petrol.*, *32*, 501–537, 1991.
- White, R. S., D. McKenzie, and R. K. O’Nions, Oceanic crustal thickness from seismic measurements and rare earth element inversions, *J. Geophys. Res.*, *97*, 19,683–19,715, 1992.
- Yang, H. J., R. J. Kinzler, and T. L. Grove, Experiments and models of anhydrous, basaltic olivine-plagioclase-augite saturated melts from 0.001 to 10 kbar, *Contrib. Mineral. Petrol.*, *124*, 1–18, 1996.

K. Grönvöld, Nordic Volcanological Institute, Grensásvegur 50, 108 Reykjavík, Iceland. (karl@norvol.hi.is)

F. Hilton and D. McKenzie, Bullard Laboratories, Department of Earth Sciences, Madingley Road, Cambridge, CB3 0EZ, UK. (maclenna@esc.cam.ac.uk; mckenzie@esc.cam.ac.uk)

J. Maclennan, Laboratoire de Géosciences Marines, Institut de Physique du Globe de Paris, F-75005 Paris, France. (maclenna@ipgp.jussieu.fr)

N. Shimizu, Department of Geology and Geophysics, Woods Hole Oceanographic Institution, Woods Hole, MA 02543, USA. (nshimizu@whoi.edu)